Chromatic Dispersion Compensation Using a Virtually Imaged Phased Array (VIPA)

by

Christopher Lin

Submitted to the Department of Electrical Engineering and Computer Science
in partial fulfillment of the requirements of the degree of
Master of Engineering in Electrical Engineering

at the

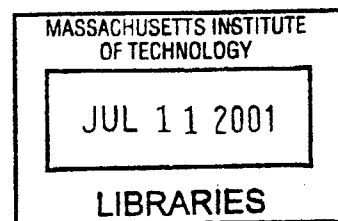MASSACHUSETTS INSTITUTE OF TECHNOLOGY

June 2000

Signature of Author..
Department of Electrical Engineering and Computer Science
May 12, 2000

Certified by..
Hermann A. Haus Institute Professor of Electrical Engineering
Thesis Supervisor

Accepted by...
Arthur C. Smith
Chairman, Department Committee on Graduate Students

Chromatic Dispersion Compensation Using a Virtually Imaged Phased Array (VIPA)

by

Christopher Lin

Submitted to the Department of Electrical Engineering and Computer Science
on May 12, 2000 in partial fulfillment of the requirements for the degree of
Master of Engineering in Electrical Engineering

Abstract

Chromatic dispersion limits the performance of modern optical communications systems. Chromatic dispersion causes pulse broadening over long transmission distances, which constrains the bit-rate.

A Virtually Imaged Phased Array (VIPA) in conjunction with a lens and mirror compensates for distortion induced by chromatic dispersion. The VIPA compensator processes all wavelength-division-multiplexed channels in a fiber in parallel. A VIPA is generated from multiple reflections within an etalon that is partially transmissive on one surface and perfectly reflective on the other (aside from an anti-reflection coated input/output window). The virtual images interfere to produce angular dispersion, which is converted to chromatic dispersion by a lens and mirror.

This thesis uses numerical simulation to explore and evaluate the performance of different VIPA compensator configurations. Results demonstrate that the system mirror can be designed to correct arbitrary chromatic dispersion, and that insertion loss is independent of dispersion bias, though mode-shaping through etalon transmissive coating design can permit wide bandwidth and low insertion loss systems.

Thesis Advisor: Hermann A. Haus

Title: Institute Professor

2

Acknowledgements

I would like to thank Dr. Masataka Shirasaki for everything he has shared with me. He always assumed the best in me and always challenged me to solve problems armed with only my wits and a piece of chalk. Above all, he taught me how to use what I already know to answer my own questions.

Being in Professor Hermann A. Haus's company was a pure pleasure. I will forever be amazed at his ability to comprehend anything nearly instantaneously. He always has questions to ask. He showed me that true understanding is the ability to ask questions. I thank him for teaching me how to ask my own questions and for the opportunity to work with him.

I thank Patrick Chou, Juliet T. Gopinath, and Jeremy D. Sher for taking the time to help me with my thesis presentation and text. I also thank Afsana N. Akhter, with whom I worked last year, for being a great co-worker and for paving the way for my own thesis.

I thank Dr. Simon Cao, Dr. Charlene Yang, and Jay Ma for fruitful discussions and insights. I also thank the members of the Optics and Devices Group for their wonderful weekly presentations.

Finally, I extend my heartfelt thanks to my family, friends, and teachers who have taught me so much and made my life so joyful.

Table of Contents

List of Figures

List of Tables

Figure 1-1: Schematic of VIPA compensator

1.0 Introduction

Chromatic dispersion in optical fibers limits the bandwidth or transmission distance of high performance communications systems. Chromatic dispersion arises from the physical reality that different wavelengths travel at different group velocities through an optical fiber. Although this effect is small, the resultant pulse broadening becomes substantial over long distances or at high bit-rates. Pulses that will spread need to be spaced farther apart than pulses that will not spread, to avoid pulse overlap and subsequent detection errors. Greater space between pulses translates to lower bit-rate. A Virtually Imaged Phased Array (VIPA)[1] provides a low loss, compact, and tunable solution to the problem of chromatic dispersion compensation [1,2]. The VIPA compensator also simultaneously processes all wavelength-division-multiplexed channels in an optical fiber.

---

1. The Virtually Imaged Phased Array (VIPA) was invented by Dr. Masataka Shirasaki at Fujitsu Laboratories, Japan, in 1995.

1.1 Current technology

The conventional method of compensating for chromatic dispersion is to use Dispersion Compensating Fiber (DCF) [3]. Standard optical fibers have positive dispersion, whereas DCF has negative dispersion. However, the length of DCF needed to compensate a given amount of chromatic dispersion is comparable to the length of the fiber generating the chromatic dispersion, on the order of 25 km of DCF per 100 km of standard single-mode fiber. This large length of DCF eliminates the possibility of a compact compensator. In addition, DCF is lossy and introduces its own distortion through a large nonlinear effect, due to its narrow core size. Finally, DCF is not tunable, which hampers the flexibility of systems incorporating such fibers. A VIPA based system can produce large, tunable chromatic dispersion with low loss and no nonlinear effects in a compact module.

Alternative technologies based on diffraction gratings or Bragg grating filters [4] have other limitations. Diffraction gratings with enough angular dispersion to be useful have polarization dependent loss. Bragg grating filters provide chromatic dispersion only in discrete steps. They are also very long, on the order of tens of meters. A compensator built with a VIPA has no polarization dependent loss and provides continuous dispersion over wavelength.

1.2 VIPA description

A VIPA is generated by an etalon, made of air or glass, with reflection coatings on both sides. The reflective side has a 100% reflection coating except for an input/output window which is anti-reflection coated. The transmissive side is only partially reflective with a coating that can have an arbitrary functional form (this research considers constant, linear amplitude (parabolic intensity), and multi-level transmissivity profiles).
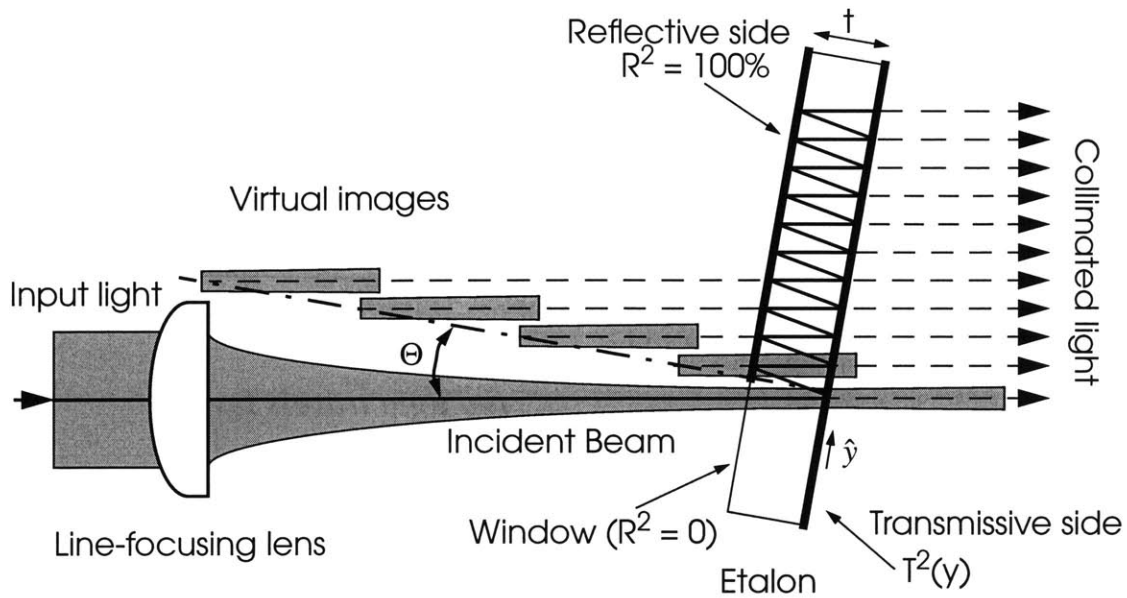
Figure 1-2: Virtually imaged phased array generation

The input is a Gaussian beam from a single-mode optical fiber. This light is first allowed to diverge and is then collimated using a spherical lens. It is then line focused, through a semi-cylindrical lens, into the VIPA plate. The etalon is tilted at an angle Θ so that the multiple reflections within the etalon create an array of virtual images that interfere on the etalon's transmissive surface (see FIGURE 1-2). Notably, these virtual images are in phase since they all originate from the same initial image. This fact is central to determining the wavelength dependent transmission angle Φ (presented in SECTION 2).

A lens and mirror complete the system. The lens transforms the etalon's angular dispersion into a lateral translation in the focusing lens's focal plane, where the mirror is placed. The reflection from a flat mirror back through the lens and onto the etalon's transmissive surface is flipped and shifted. The shift depends on the initial angular dispersion, which is dependent on wavelength. This shift generates negative chromatic dispersion because different wavelengths travel different path lengths within the etalon while returning to the optical fiber. Blue light is

blue light travels more

red light travels less
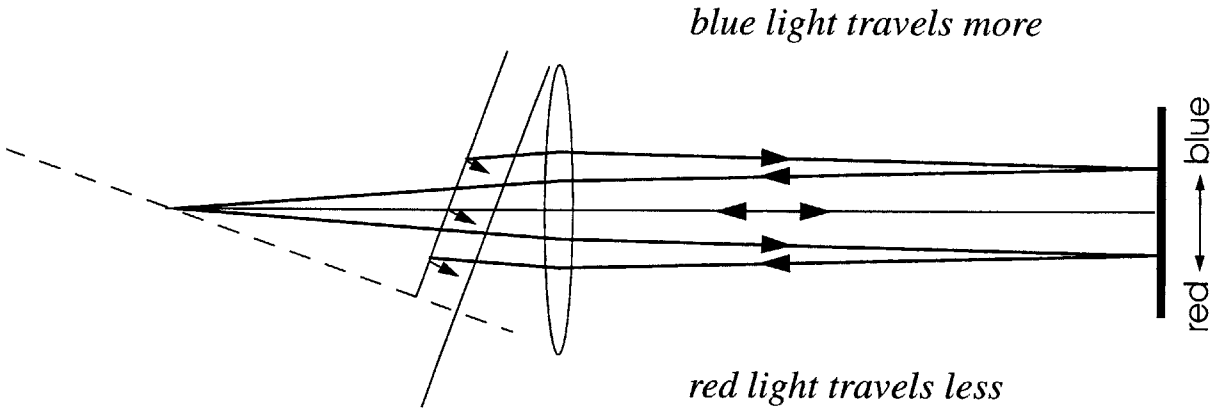
Figure 1-3: Light paths for different wavelengths

deflected upwards and is reflected farther up the etalon. In order to exit the etalon through the window and return to the optical fiber, it must bounce back and forth between the etalon's mirrors more times than red light; it therefore encounters a longer path length (see FIGURE 1-3).[2] By changing the shape of the mirror, this basic effect can be magnified. By changing the detailed profile of the mirror, the functional form or shape of the dispersion can be modified. Finally, by changing the distance between the etalon and lens (and keeping the lens-mirror spacing fixed), the dispersion can be tuned.

The etalon can be thought of as a mode transformer. It takes the mode of an optical fiber (a Gaussian beam) and transforms it into some transmission mode on its transmissive surface. The lens and mirror merely feed a modified version of this transmission mode back into the etalon. By reversing the operation of the etalon, the ideal mode that would produce a Gaussian beam at the optical fiber can be defined. With this definition, the integral of the overlap between the reflection mode and the ideal mode yields the coupling loss of the modes as well as the group delay. The

---

2. The ray trace in FIGURE 1-3 only shows what happens to the virtual image source along the lens axis. As will be shown in SECTION 2, the light path is independent of the initial virtual image. Therefore, following only one image completely describes the compensator's operation.

dispersion is the derivative of the group delay with respect to wavelength. The ideal mode is the conjugate of the transmission mode. Since the dispersion comes from the shift of the reflection mode relative to the ideal mode, greater shift means more loss since the overlap integral is smaller if the two modes are spaced farther apart.

A VIPA can also be used to perform wavelength division multiplexing/de-multiplexing. References [5]-[7] describe this function and provide relevant insight into the chromatic dispersion compensation application.

1.3 Design considerations

Seven variables determine the performance specifications of the VIPA chromatic dispersion compensator. These are the input beam waist w_o, the input angle (Θ in air and θ in etalon), the etalon's thickness t, the etalon's index of refraction n, the width of the transmission mode (related to the transmissivity profile of the etalon's transmissive surface $T(y)$), the focal length of the lens f, and the shape of the mirror $c(y)$. These variables determine the *dispersion bias*,[3] the shape of the dispersion profile, the insertion loss, the bandwidth, and the free spectral range (FSR) of the VIPA compensator.

Of these five performance specifications, two involve no substantial trade-offs: dispersion shape and FSR. Shaping the dispersion profile by changing $c(y)$ will not greatly affect the bandwidth as long as the dispersion bias is unchanged. The bandwidth may be improved or degraded depending on whether the dispersion at the band edges is decreased or increased respectively.

---

3. In general, the dispersion generated by the VIPA compensator will not be constant over wavelength. In order to provide a useful reference for comparison between different VIPA compensator configurations, dispersion bias has been defined as the dispersion at the center wavelength of the center WDM channel. Furthermore, the center wavelength is defined as the wavelength in the center of the -1 dB band. This wavelength may be different from the undeflected wavelength whose transmission angle Φ is equal to Θ. Subsequent sections will further develop this point.

Since the FSR is set by industry standard (100 GHz or 0.8 nm), the values of t and n must be chosen to ensure that the transmission angles of wavelengths differing by an integer multiple of the FSR are identical (see SECTION 2).

The index of refraction is the overall performance limiting factor. The etalon thickness and index of refraction determine the FSR, but larger n greatly increases the potency of the compensator. As will be seen in SECTION 2, the compensator's dispersive ability is proportional to the fourth power of the etalon's index of refraction.

Having discussed the dispersion shape and FSR, there are only three fundamental metrics left to consider: insertion loss, bandwidth, and dispersion bias. In fact, the only trade-off will be between bandwidth and dispersion. As will be shown, the insertion loss is independent of both. Herein lies perhaps the most important advantage of the VIPA compensator over DCF. The loss (in dB) of DCF increases linearly with dispersion. For large amounts of dispersion, the VIPA compensator will undoubtedly have less loss than DCF. The price for this freedom is bandwidth narrowing. DCF has no bandwidth limitations. The transmission spectrum of DCF over a single WDM channel is completely flat.

Characteristic waist w_0

The input to the VIPA compensator is assumed to be the output of a single-mode optical fiber. The amplitude profile can be approximated by a Gaussian. To a first-order approximation, the input window loss is minimized when the beam is line-focused onto the transmissive surface of the etalon along the same line where the highly reflective coating is applied on the reflective surface (see FIGURE 1-4). Any other point of focus will increase the input window loss or first reflection loss by more than it reduces the other.
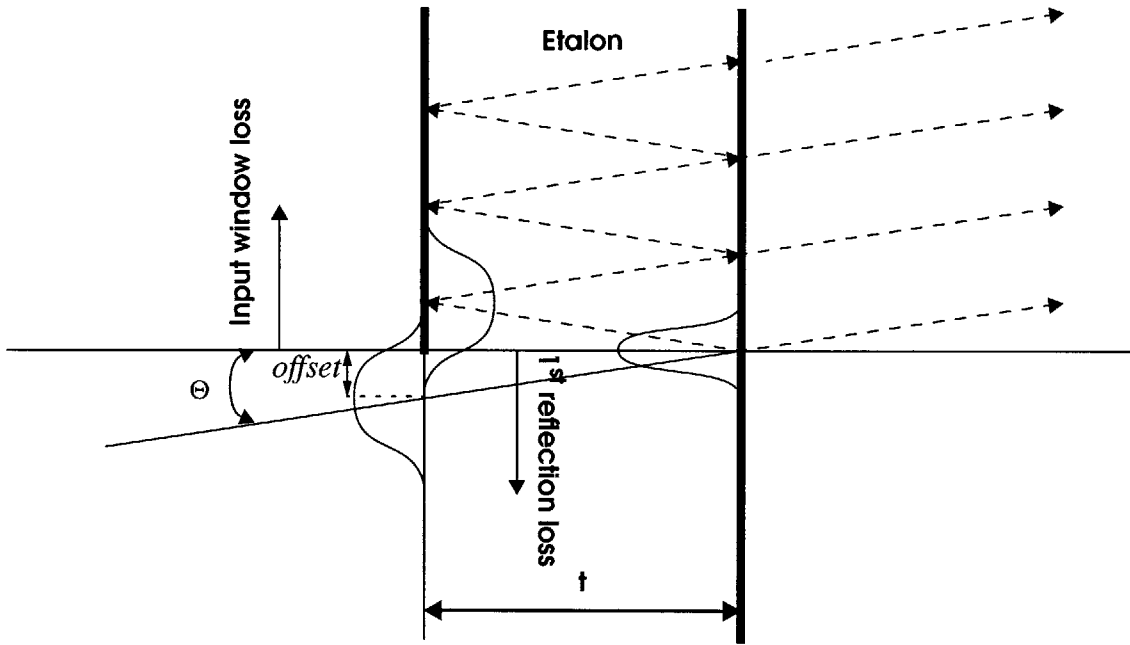
Figure 1-4: Initial window loss

The waist that minimizes the initial window loss at the undeflected wavelength is the most narrow waist at the etalon's reflective surface (see EQUATION 1.1). The beam waist of the power profile is equal to this value divided by $\sqrt{2}$. Using trigonometry, the *offset* can be computed from the refractive index adjusted incident angle θ in the etalon. This offset is the distance between the beam center and the reflective surface coating discontinuity. All of the power that falls above the coating is lost.

Minimal window loss characteristic waist computation

$$w^2 = w_0^2\left[1 + \left(\frac{\lambda_n z}{\pi w_0^2}\right)^2\right] \qquad [1.1]$$

$$\frac{dw}{dw_0} = 2w_0 - \frac{2\lambda_n^2 z^2}{\pi^2 w^2} = 0$$

$$w_0 = \sqrt{\frac{\lambda_n z}{\pi}}$$

16

Estimated window loss[4]

$$offset = t \cdot \tan\theta$$

$$windowLoss = \frac{1 - erf\left(\dfrac{offset}{powerWaist}\right)}{2} \qquad [1.2]$$

Input angle Θ

Smaller incident angles increase the dispersion bias but also increase the window and etalon losses, since more initial power is cut off and more power can escape during subsequent reflections. The bandwidth also decreases with decreasing angle of incidence since larger dispersion means the reflected mode is displaced farther from the ideal mode and therefore does not couple as well.

Transmission profile $T(y)$

The transmission profile shapes the VIPA modes (transmission and reflection). Wider modes overlap better at the band edges (higher bandwidth), but sacrifice dispersion bias (see SECTION 2). The presence of non-centralized peaks in the mode profile enhances bandwidth, and symmetric modes have lower insertion loss than asymmetric modes.

Focal length f and mirror shape $c(y)$

The focusing lens converts the VIPA's angular dispersion into chromatic dispersion by mapping the different etalon transmission angles to different positions in the focal plane where the mirror is located, and therefore to different traveling distances. Larger f or smaller radius of curvature results in higher dispersion but lower bandwidth, since the displacement between the reflection mode and the ideal mode will increase more rapidly over wavelength with larger f or smaller radius of curvature.

---

4. This can also be computed numerically. SECTION 4-2 details the numerical computation.

Other considerations

In addition to providing a quantitative way of evaluating insertion loss, bandwidth, and dispersion, this thesis provides insight into engineering the shape of the VIPA mirror. The VIPA chromatic dispersion compensator tends to produce greater negative dispersion for longer wavelengths. This trend may or may not have anything to do with the dispersion to be compensated. To be truly useful, there must be an easy way to design a mirror to produce a compensation profile that is matched to the particular application. In the tunable case, this mirror shape will have to be a compromise over the range of operation unless the mirror can also be tuned.

One final consideration is the deviation of compensation of the system for different channels. The VIPA is optimized for the center channel in a WDM band. Other channels have slightly different wavelengths and therefore react differently to the various components of the VIPA compensator. Other channels also have different dispersion. The VIPA compensator corrects each channel in the same way. All channels are improved, but only the center channel is completely compensated.

2.0 Theoretical Dispersion

While the insertion loss of the VIPA compensator is hard to predict analytically, the dispersion performance can be readily described using straightforward ray optics.
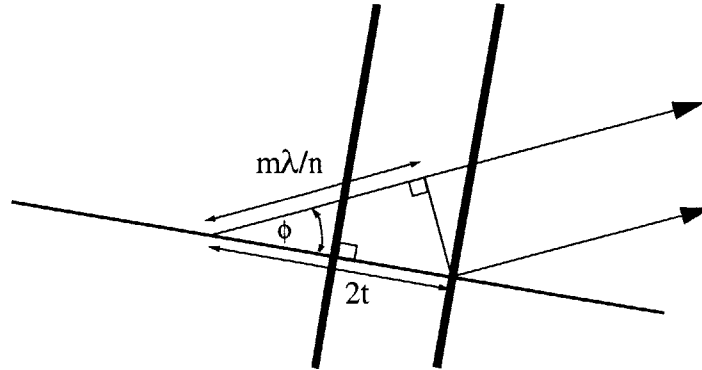
Figure 2-1: Transmission angle in etalon (ϕ)

As mentioned in SECTION 1.2, the virtual image sources of the VIPA are all in phase. This reduces the calculation of the wavelength dependent transmission angle to an antenna problem. The differential path length between two sources must be an integer multiple of the index adjusted wavelength in order to have constructive interference:

$$\Phi \approx n\phi, \quad \cos\phi = \frac{m\lambda}{2nt} \qquad \Rightarrow \qquad \frac{d\Phi}{d\lambda} \approx -\frac{n^2}{\lambda\Phi} \qquad [2.1]$$

The FSR is also implicitly contained in EQUATION 2.1. When λ is varied by an integer multiple of the FSR, Φ must remain constant. Therefore, $(m - k)(\lambda_m + k \cdot FSR)$ where k is some integer must stay fairly constant as k is varied over the integers. This constrains the value of nt, since nt determines m when Φ, λ_m, and the FSR are fixed.

The light path from the virtual image along the lens axis to the mirror and back can be approximated by EQUATION 2.2, where a is the distance between the axial or center virtual image and the lens, and $c(y)$ is the shape of the mirror (see FIGURE 2-2). FIGURE 2-2 is somewhat mis-
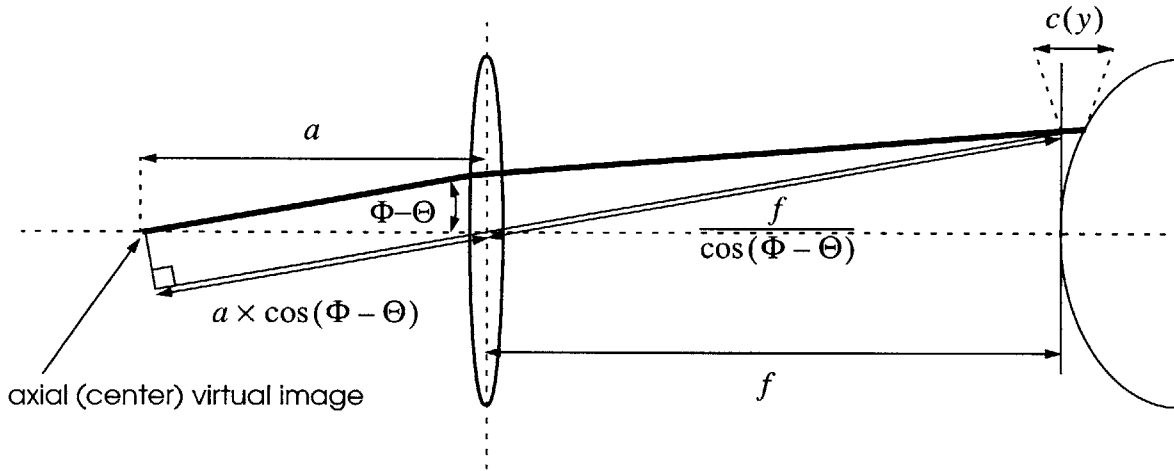
Figure 2-2: Light path

leading because the angle (Φ–Θ) is too small to be accurately depicted. In the limit where (Φ–Θ)

is very small:

$$lightPath = 2\left[a \cdot \cos(\Phi - \Theta) + \frac{f}{\cos(\Phi - \Theta)} + c(y)\right] \qquad [2.2]$$

$$y = f(\Phi - \Theta)$$

The system geometry demonstrates that this light path applies to all light of a specific

wavelength from each of the virtual images. FIGURE 2-3 shows the undeflected case, but the result

is general. The optical paths to the right of the lens are all equal because of the effect of the lens,

and the optical paths to the left of the lens are equal because the sum of the distances between any

complementary pair of images and the lens is always $2a$.

The phase advance for each wavelength is:

$$phaseChange = \frac{2\pi}{\lambda}lightPath$$

$$phaseChange = \gamma \approx \frac{2\pi}{\lambda}[2(f + a) + (f - a)(\Phi - \Theta)^2 + 2c(y)] \qquad [2.3]$$

20
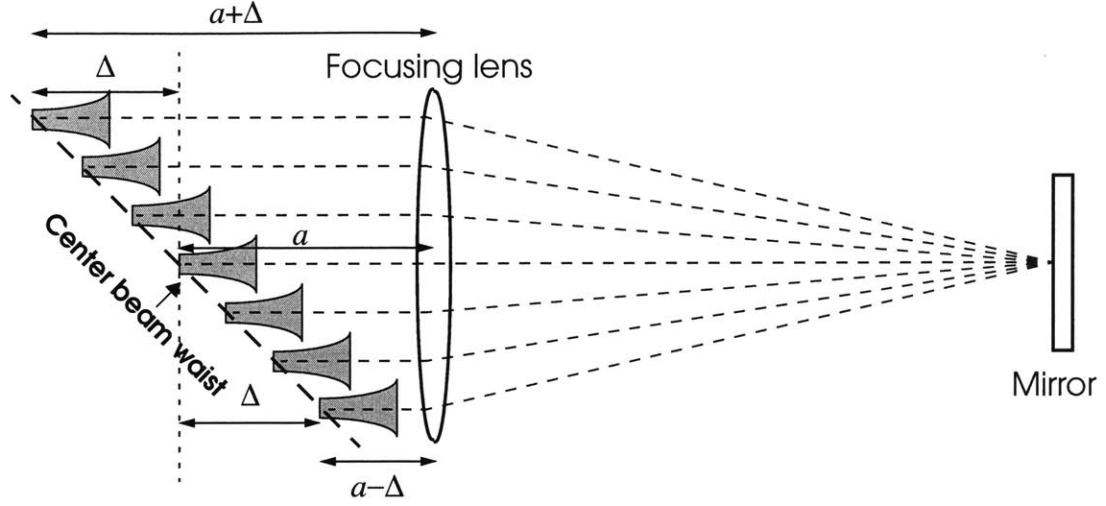
Figure 2-3: Light paths of complementary virtual images

The derivative of γ with respect to ω yields the group delay:[5]

$$groupDelay = G = \frac{d\gamma}{d\omega} = \frac{-\lambda^2}{2\pi c}\frac{d\gamma}{d\lambda}$$

$$G = \frac{-2\lambda}{c}\left[(f-a)(\Phi-\Theta) + h(y)\frac{dy}{d\Phi}\right]\frac{d\Phi}{d\lambda}$$

$$h(y) = \frac{d}{dy}c(y)$$

$$G = \frac{2n^2}{c\Phi}\{(f-a)(\Phi-\Theta) + fh(y)\} \qquad [2.4]$$

Finally, the derivative of the group delay with respect to wavelength is the dispersion:

$$dispersion = D = \frac{dG}{d\lambda} = -\frac{2n^4}{c\lambda\Phi^3}\left[(f-a)\Phi + f^2\Phi\frac{d}{dy}h(y) - fh(y)\right] \qquad [2.5]$$

This expression explains why wider transmission modes have lower dispersion. Wider modes are centered farther up the etalon. This increases the value of a which decreases the magnitude of the dispersion. Also, the dispersion is proportional to n^4, which calls for high-n etalons.

---

5. The first term is ignored since it is roughly constant over the WDM channel and only the change in group delay is important (see APPENDIX B).

21

3.0 Mirror Design

The mirror placed in the focal plane of the focusing lens has a profound effect on the dispersion produced by the VIPA compensator. Placing a convex mirror, for example a simple parabolic mirror, in the focal plane will augment the overall dispersive effect. More complicated mirrors can shape the dispersion as a function of wavelength. For example, the natural tendency of the VIPA is for longer wavelengths to have greater dispersion. The correct mirror can cancel this tendency and provide constant dispersion over the range of operation.

3.1 Parabolic mirror

For a parabolic mirror, EQUATION 2.5 yields:

$$c(y) = \frac{y^2}{2r}$$

$$D = -\frac{2n^4}{c\lambda\Phi^3}\left\{(f-a)\Phi + \frac{f^2\Theta}{r}\right\}$$

This dispersion can vary over a 0.6 nm band by nearly an order of magnitude.

3.2 Constant dispersion mirror

A more interesting case is uniform dispersion over the WDM channel. Since λ changes very slowly over the band, the dispersion will be very uniform if the multiplicand in brackets in EQUATION 2.5 is proportional to Φ^3:

$$(f-a)\Phi + f^2\Phi\frac{d}{dy}h(y) - fh(y) = K_0\Phi^3 \qquad \Rightarrow \qquad D_0 = -\frac{2n^4K_0}{c\lambda}$$

22

By assigning the initial condition $h(0) = 0$ and solving this differential equation in y, the shape of the required mirror can be derived:

$$\Phi = \frac{y}{f} + \Theta$$

$$f^2\left(\frac{y}{f} + \Theta\right)\frac{d}{dy}h_0(y) - fh_0(y) = K_0\left(\frac{y}{f} + \Theta\right)^3 - (f - a)\Theta$$

$$h_0(0) = 0$$

$$h_0(y) = \frac{K_0}{2f^4}y^3 + \frac{3K_0\Theta}{2f^3}y^2 + \frac{K_0\Theta^2 - (f - a)}{f^2}y$$

$$\frac{d}{dy}h_0(y) = \frac{3K_0}{2f^4}y^2 + \frac{3K_0\Theta}{f^3}y + \frac{K_0\Theta^2 - (f - a)}{f^2}$$

$$c_0(y) = \frac{K_0}{8f^4}y^4 + \frac{K_0\Theta}{2f^3}y^3 + \frac{K_0\Theta^2 - (f - a)}{2f^2}y^2$$
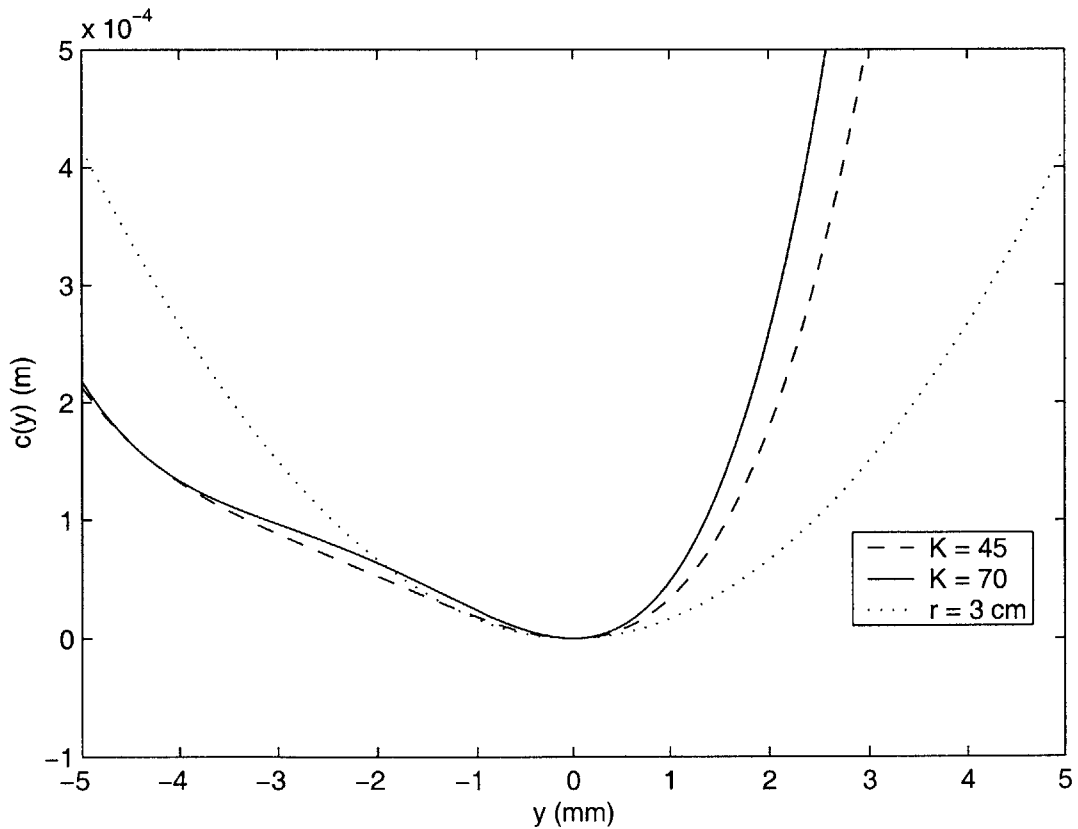
Figure 3-1: Shape of two constant dispersion mirrors (K=45, 70)

3.3 Arbitrary Dispersion Mirrors

More complicated mirrors can produce arbitrary dispersion profiles. The process is indirect since the mirror shape is most easily described as a function of y which is proportional to $\sqrt{\lambda}$. The basic method of computing these mirror shapes as a function of y begins with assuming a proportionality relationship, as in the previous section for the constant dispersion case. Here, a few of the lower-order cases are presented.

First-order mirror

$$(f-a)\Phi + f^2\Phi\frac{d}{dy}h(y) - fh(y) = K_1\Phi^3 y \qquad \Rightarrow \qquad D_1 = -\frac{2n^4 K_1 y}{c\lambda}$$

$$h_1(y) = \frac{K_1}{3f^4}y^4 + \frac{5K_1\Theta}{6f^3}y^3 + \frac{K_1\Theta^2}{2f^2}y^2$$

$$c_1(y) = \frac{K_1}{15f^4}y^5 + \frac{5K_1\Theta}{24f^3}y^4 + \frac{K_1\Theta^2}{6f^2}y^3$$

Second-order mirror

$$(f-a)\Phi + f^2\Phi\frac{d}{dy}h(y) - fh(y) = K_2\Phi^3 y^2 \qquad \Rightarrow \qquad D_2 = -\frac{2n^4 K_2 y^2}{c\lambda}$$

$$h_2(y) = \frac{K_2}{4f^4}y^5 + \frac{7K_2\Theta}{12f^3}y^4 + \frac{K_2\Theta^2}{3f^2}y^3$$

$$c_2(y) = \frac{K_2}{24f^4}y^6 + \frac{7K_2\Theta}{60f^3}y^5 + \frac{K_2\Theta^2}{12f^2}y^4$$

Third-order mirror

$$(f-a)\Phi + f^2\Phi\frac{d}{dy}h(y) - fh(y) = K_3\Phi^3 y^3 \qquad \Rightarrow \qquad D_3 = -\frac{2n^4 K_3 y^3}{c\lambda}$$

$$h_3(y) = \frac{K_3}{5f^4}y^6 + \frac{9K_3\Theta}{20f^3}y^5 + \frac{K_3\Theta^2}{4f^2}y^4$$

$$c_3(y) = \frac{K_3}{35f^4}y^7 + \frac{3K_3\Theta}{40f^3}y^6 + \frac{K_3\Theta^2}{20f^2}y^5$$

$$(f-a)\Phi + f^2\Phi\frac{d}{dy}h(y) - fh(y) = K_4\Phi^3y^4 \qquad \Rightarrow \qquad D_4 = -\frac{2n^4K_4y^4}{c\lambda}$$

$$h_4(y) = \frac{K_4}{6f^4}y^7 + \frac{11K_4\Theta}{30f^3}y^6 + \frac{K_4\Theta^2}{5f^2}y^5$$

$$c_4(y) = \frac{K_4}{48f^4}y^8 + \frac{11K_4\Theta}{210f^3}y^7 + \frac{K_4\Theta^2}{30f^2}y^6$$

Table 3-1: Coefficients of mirror shape, c(y)

Order (n)	$y^{(n+4)}$	$y^{(n+3)}$	$y^{(n+2)}$
0	$K_0 / 8f^4$	$K_0\Theta / 2f^3$	$[K_0\Theta^2 - (f-a)] / 2f^2$
1	$K_1 / 15f^4$	$5K_1\Theta / 24f^3$	$K_1\Theta^2 / 6f^2$
2	$K_2 / 24f^4$	$7K_2\Theta / 60f^3$	$K_2\Theta^2 / 12f^2$
3	$K_3 / 35f^4$	$3K_3\Theta / 40f^3$	$K_3\Theta^2 / 20f^2$
4	$K_4 / 48f^4$	$11K_4\Theta / 210f^3$	$K_4\Theta^2 / 30f^2$

The most straightforward way to use these equations is to map the desired dispersion as a function of wavelength to the desired dispersion as a function of y. Then, a linear least squares superposition of these mirrors would yield the desired profile.

$$\cos\left(\frac{\Phi}{n}\right) = \frac{m\lambda}{2nt} \qquad \Rightarrow \qquad 1 - \frac{\Phi^2}{2n^2} \approx \frac{m\lambda}{2nt} \qquad \Rightarrow \qquad \Phi \approx n\sqrt{2 - \frac{m\lambda}{nt}}$$

$$y \approx f(\Phi - \Theta)$$

$$y \approx f\left(n\sqrt{2 - \frac{m\lambda}{nt}} - \Theta\right)$$

As an example, assume that some application requires dispersion compensation of -1,700 ps/nm at 1550.0 nm with a slope of -100 ps/nm^2. TABLE 3-2 lists the K_n coefficients for successively higher orders of linear least squares approximations to the reference line. FIGURE 3-2 plots the results. In this particular example, the 3rd and 4th order terms are not needed.[6]

Table 3-2: Linear dispersion mirror

Order	K_0	K_1	K_2	K_3	K_4
0	37.7	-	-	-	-
1	37.6	-879	-	-	-
2	37.7	-925	-212,000	-	-
3	37.7	-925	-212,000	0	-
4	37.7	-925	-212,000	0	0
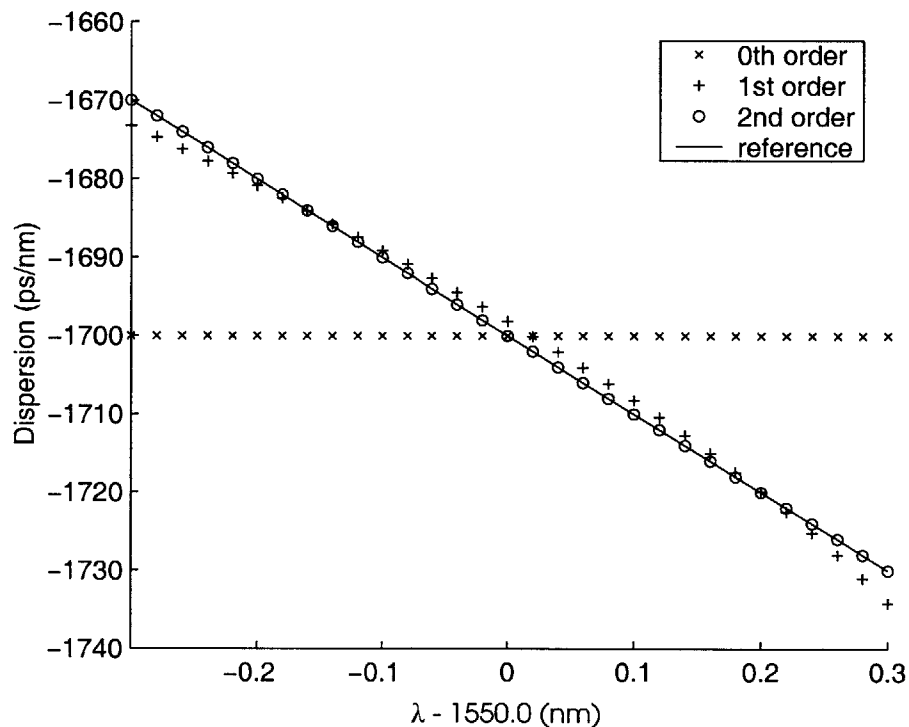
Figure 3-2: Linear dispersion mirror

6. The dispersion over a single WDM channel is essentially constant. The usefulness of arbitrary dispersion mirrors turns out to be in so-called "dispersion slope compensators" (also built around a VIPA) which produce different dispersion for different WDM channels. The VIPA compensator discussed in this work corrects each WDM channel in exactly the same way. Further discussion of dispersion slope compensators is beyond the scope of this thesis.

4.0 Numerical Model

The VIPA compensator is a simple device. Its dispersion performance is accurately predicted by ray optics. Only basic diffraction-limit optics theory is needed to fully describe the VIPA compensator's operation. Haus's text provides an excellent description of these theoretical tools [8]. For this thesis, this diffraction limit model was programmed using MATLAB™ in order to sketch the compensator's transmission spectrum. The simulation also calculated the dispersion performance in order to confirm the ray optics results.

4.1 Parameters

Table 4.1: List of parameters

Parameter	Symbol
index of etalon	n
etalon thickness	t
wavelength in free space	λ
beam waist	w_0
incident angle in air, in etalon	Θ, θ
transmission angle in air, in etalon	Φ, ϕ
focal length of focusing lens	f
distance between etalon and lens	l
distance between center virtual image and lens	a
transmission coating	$T(y)$
shape of mirror	$c(y)$

4.2 Inside the etalon

Since the VIPA is operating in the paraxial limit, the Fresnel diffraction integral describes the behavior of the input light within the device. Application of the Fresnel diffraction integral is equivalent to multiplication by a phase factor in the frequency domain.

Fresnel diffraction equations[7]

$$u(y, z) = \frac{j}{\lambda z} \exp(j k_{glass} z) \int_{-\infty}^{\infty} u_0(y_0) \exp\left(-j \frac{k_{glass}}{2z}(y - y_0)^2\right) dy_0$$

$$U(k_y, z) = U_0(k_y) \exp(j k_{glass} z) \exp\left(-j \frac{k_y^2}{2 k_{glass}} z\right)$$

Phase factor for forward propagation:

$$phaseFactor = P(z) = \exp(j k_n z) \exp\left(-j \frac{k_y^2}{2 k_n} z\right)$$

Using the phase factor with $z = -t$ on an ideal focused Gaussian beam, with linear phase offset due to the tilt Θ of the VIPA compensator, the unobstructed input just before the reflective surface of the etalon can be calculated. If the input light before incidence is normalized, with normalization constant A, the window loss can be computed. The result of the integral must be squared since power will be lost through this mechanism on the return path as well. Subsequently, the phase factor with $z = +t$ and reflection factors (R_L, left or reflective side, and R_R, right or transmissive side) are repeatedly applied to obtain the complete field profile on the etalon's transmissive surface, T_{Total}.

Window loss

$$windowLoss = 1 - \left(\int_{-\infty}^{\infty} |U_{InitialLeft}|^2 dy\right)^2$$

---

7. All of the following formulae were implemented using their discrete equivalents. This introduced some numerical complications that are not central to the theory. For clarity, pertinent commentary is presented only in the code included in APPENDIX C. Also for clarity, λ always refers to the free space wavelength. The refractive index will always be carried explicitly throughout this work.

Iterative propagation calculation

$$U_{InitialLeft} = (1 - R_L)F^{-1}\left\{ F\left\{ A\exp\left(-\frac{(y - y_0)^2}{w_0^2} \right) \right\} P(-t)L_{Phase} \right\}$$

$$L_{Phase} = \exp(j(y - y_0)k_{glass}\sin(\theta))$$

$$A = \sqrt{\frac{1}{\sqrt{\int_{-\infty}^{\infty} \left| \exp\left(-\frac{(y - y_0)^2}{w_0^2} \right) \right|^2 dy}}}$$

$$U_{1R} = BF^{-1}\{F\{U_{InitialLeft}\}P(t)\}$$

$$B = \sqrt{\frac{1}{\sqrt{\int_{-\infty}^{\infty} \left| F^{-1}\{F\{U_{InitialLeft}\}P(t)\} \right|^2 dy}}}$$

$$U_{1L} = F^{-1}(\{F\{R_R U_{1R}\}P(t)\})$$

$$U_{2R} = F^{-1}(\{F\{R_L U_{1L}\}P(t)\})$$

$$U_{Total} = \sum_{1}^{N} U_{nR}$$

After enough[8] iterations N, the U_{nR} vectors are added to yield the total field profile U_{Total} before transmission through the etalon's transmissive surface. This sum is multiplied by $T(y)$, where $T(y)$ is the transmissivity of the transmissive surface, to yield T_{Total}. Each reflection results in power loss through the window as well as deviation from the virtual image ideal (see FIGURE 4-1). The total etalon loss is calculated by normalizing the input power after the initial window loss, using normalization constant B, and evaluating the final transmitted power. Again, this result must be squared to account for the return loss by the same mechanism.

---

8. "Enough" iterations to provide an accurate representation of U_{Total} in the constant transmissivity case is generally 400. This number depends on the overall transmissiveness of the transmissive coating. A more transmissive coating requires fewer iterations, as light is rapidly lost with each reflection. A less transmissive coating requires more.

Etalon loss

$$etalonLoss = 1 - \left(\int_{-\infty}^{\infty} |T_{Total}|^2 dy \right)^2$$
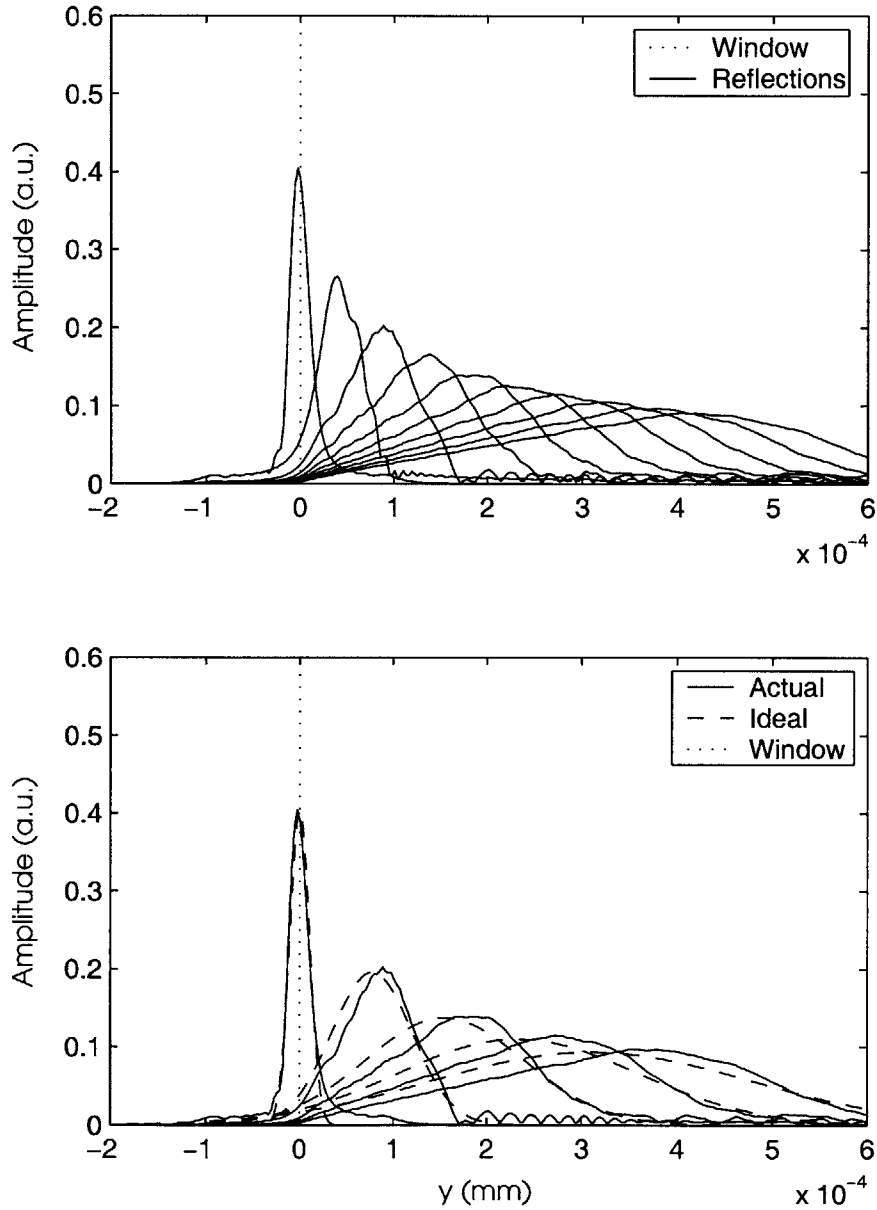
Figure 4-1: Reflections at the etalon transmissive surface.
(a) First 10 reflections (2.0 % Transmissivity, $\Theta = 2.5°$).
(b) 1st, 3rd, 5th, 7th, and 9th actual and ideal reflections.
Ideal reflections assume no window.

4.3 Lens and mirror

The effect of the lens can be determined by first calculating the Fourier transform V_{Total} of T_{Total}. Given V_{Total}, V_{Main} for the undeflected wavelength is the lobe with the highest power.[9] For the other wavelengths, V_{Main} is the lobe appropriately situated with respect to the undeflected wavelength's main lobe. V_{Main} for longer wavelengths will be the first lobe to the left of the undeflected wavelength's main lobe and V_{Main} for shorter wavelengths will be
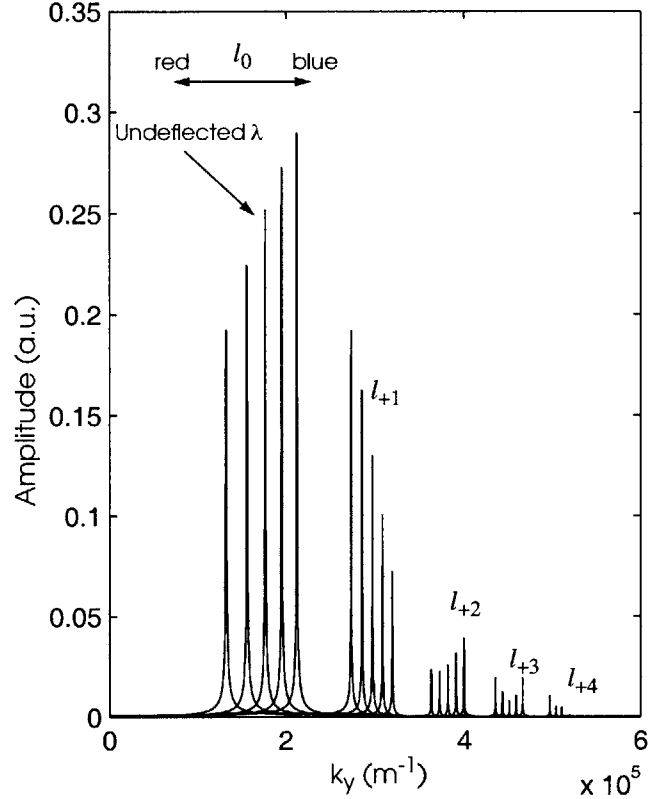
Figure 4-2: Lobes of V_{Total} in the focal plane

the first lobe to the right of the undeflected wavelength's main lobe (see FIGURE 4-2). These main lobes are referred to collectively as the l_0 lobes; other lobes have different indices.[10] By first normalizing V_{Total}, using the constant C, the residual power in V_{Main} and therefore the lobe loss can be found.[11] The inverse Fourier transform of V_{Main} yields T_{Main}, normalized with constant D. V_{Main} needs to be recalculated from T_{Main}, accounting for lens alignment and phase advance.

---

9. In general, the undeflected wavelength, defined as the wavelength propagating at $\Phi = \Theta$,will not have the least lobe loss. Predicting which wavelength will have the greatest power in its main lobe is impossible without simulation. Because the array of images in the VIPA are not actually ideal Gaussian beams, the profile V_{Total} cannot be reliably predicted analytically (see SECTION 6.1).

10. l_0 refers to the lobe with the most power. $l_{i>0}$ denotes lobes at higher transmission angles and $l_{i<0}$ denotes lobes at lower transmission angles. In FIGURE 4-2, no negative lobes exist.

11. The transmission of the etalon at the mirror has multiple lobes. The light reflected back into the device by the mirror consists of only the main lobe. The rest of the power is lost and can be computed by normalizing the total transmitted power and then subtracting the power left in the main lobe. This power is actually lost "twice", so this loss factor must be squared.

Determination of T_{Main} without lens alignment

$$V_{Total} = CF\{T_{Total}\}$$

$$C = \sqrt{\frac{1}{\int_{-\infty}^{\infty} |F\{T_{Total}\}|^2 dk_y}}$$

$$T_{Main} = DF^{-1}\{V_{Main}\}$$

$$D = \sqrt{\frac{1}{\int_{-\infty}^{\infty} |F^{-1}\{V_{Main}\}|^2 dy}}$$

Lobe loss

$$lobeLoss = 1 - \left(\int_{-\infty}^{\infty} |V_{Main}|^2 dy\right)^2$$

The focusing lens is tilted at $-\Theta$ with respect to the etalon, so that it is parallel to the colli-mating and line-focusing lenses and perpendicular to the optical fiber. The focusing lens axis is aligned with the power center of T_{Main} of the undeflected wavelength (see FIGURES 4-3 and 4-4).[12]

Now, V_{Main} can be recalculated using the phase-adjusted and centered T_{Main}. This time, a phase progression factor for the distance traveled from the light center to the mirror is included.

Power center of T_{Main}

$$center = \frac{y_0}{2} \quad such\ that \quad \int_{-\infty}^{\infty} T(y)T(y_0 - y)dy \quad is\ maximized.$$

12.The power center of T_{Main} at the undeflected wavelength should be normally incident onto the center of the lens for minimal coupling loss at the undeflected wavelength. However, this is not necessarily the optimal alignment for a given application. Changing the tilt of the lens and the position of the lens axis with respect to the etalon will move the coupling loss spectrum. Changing the position of this spectrum with respect to the other loss spectra allows trading between insertion loss and bandwidth (see figures in SECTION 5). Development of this possibility is beyond the scope of this thesis.
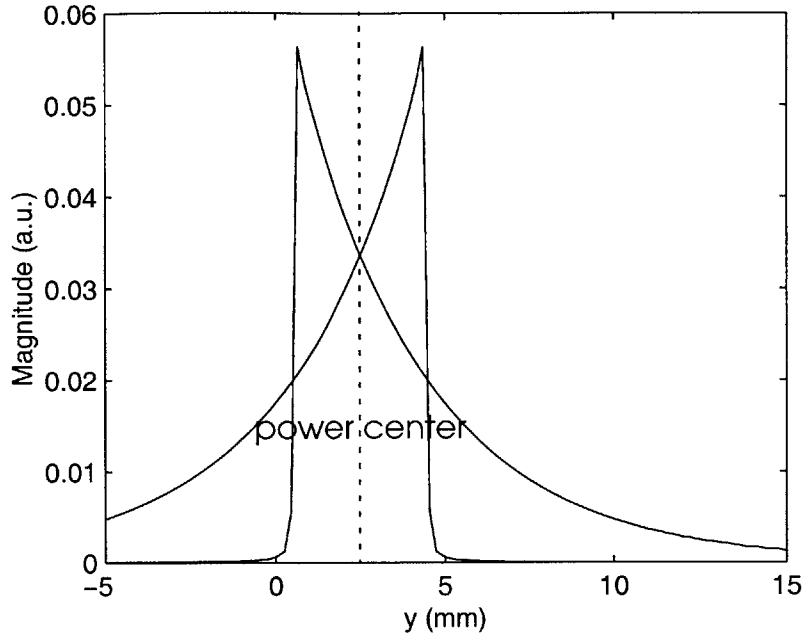
Figure 4-3: Illustration of the power center of T$_{Main}$.

T_{Main} and V_{Main} including lens alignment

$$T_{Main} = T_{Main}\exp(-jy\sin(\Theta)k_{air})$$

$$V_{Main} = F\{T_{Main}\}P_{Lens}Mirror$$

$$Mirror = \exp\left(-j2k_{air}c\left(\frac{k_y f}{k_{air}}\right)^2\right)$$
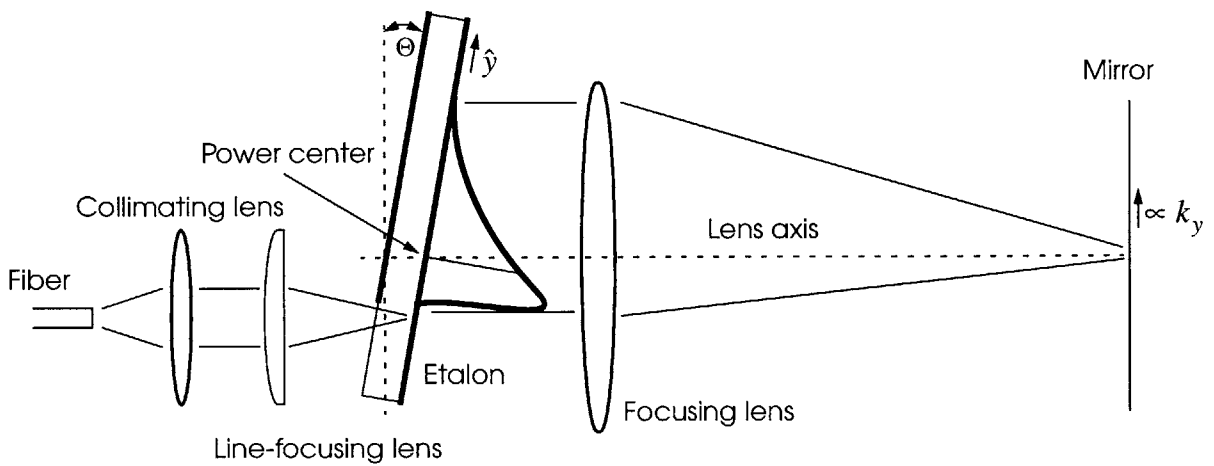
Figure 4-4: Focusing-lens alignment

Lens phase progression factor

$$P_{Lens} = \exp\left(j\left(l\cos\left(\frac{k_y}{k_{air}}\right) + \frac{f}{\cos\left(\frac{k_y}{k_{air}}\right)} \right) k_{air} \right)$$

The light reflected from the mirror will eventually couple into the output fiber. The loss through this transfer and the dispersion can be derived from the overlap integral between the reflected light R_{Main}, normalized with constant E, and the ideal fiber mode (which is the conjugate of T_{Main}). In this section, the subscript *Main* distinguishes the main mode of the relevant profile. The rest of this thesis does not require this convention; the subscript *Mode* shall always refer to the main mode.

Derivation of R_{Main}

$$R_{Main} = EF\{V_{Main}P_{Lens}\}$$

$$E = \sqrt{\frac{1}{\int\limits_{-\infty}^{\infty} |F\{V_{Main}P_{Lens}\}|^2 dy}}$$

Coupling loss and dispersion

$$overlap = \int\limits_{-\infty}^{\infty} Ideal^* R_{Main} dy$$

$$Ideal = T_{Main}^*$$

$$couplingLoss = 1 - |overlap|^2$$

$$\gamma = Phase(overlap)$$

$$groupDelay = -\frac{\lambda^2}{2\pi c}\frac{d\gamma}{d\lambda}$$

$$dispersion = \frac{d}{d\lambda}groupDelay$$

5.0 Simulation Results

The simulations evaluated three different transmissivity profiles (constant, linear, and multi-level), two mirror designs (parabolic and constant dispersion), as well as three different input angles (2.2°, 2.5°, and 2.8°). The program also explored the VIPA compensator's performance in the tunable case by varying l, the distance between the etalon and the lens. In most cases, bandwidth increases and insertion loss, dispersion bias, and the normalized dispersion standard deviation σ_n all decrease as Θ increases.[13] Also, the bandwidth is wider and the dispersion-bias smaller for less transmissive coatings, since they generate wider transmission modes (see SECTION 2). For all results, $f = 5$ cm, $n = 1.8$, $t = 800$ μm and $w_0 = 14.8$ μm (see SECTION 1.3).

The primary objective of the simulation is to generate transmission spectra for different VIPA compensator configurations. The secondary objective is to confirm the closed form ray optics dispersion formula (EQUATION 2.5). Agreement between these two techniques also provides confidence that the computed transmission spectra are correct.

The numerical dispersion calculation is subject to many computational artifacts. The simulation uses discrete approximations of continuous variables and functions. This naturally introduces noise-like errors. The phase of small complex numbers is especially sensitive to these fluctuations.[14] Finally, derivatives tend to amplify the effects of random errors. The way around these complications is to perform some kind of averaging. The simulation implements this corrective action in the difference equation used to compute the group delay from the phase γ.

---

13. Transmission spectrum clipping occurs at $\Theta = 2.8°$ because secondary lobes are not as well suppressed as they are in smaller angles (see SECTION 6.2). This effect runs counter to the expected trend that bandwidth increase as Θ increases, but it only appears when the bandwidth is already large (around 0.4 nm).
14. This error mechanism is influential at the transmission band edges where the overlap integral between the transmission and reflection modes is small. All of the major disagreement between the theory and simulation occurs in these high-loss regions (see following figures).

$$G = \frac{-\lambda^2 d\gamma}{2\pi c\, d\lambda} \qquad \Rightarrow \qquad G = \frac{-\lambda^2}{2\pi c}\left(\frac{\gamma(\lambda_{n+1}) - \gamma(\lambda_n)}{\lambda_{n+1} - \lambda_n}\right) = \frac{-\lambda^2}{2\pi c}\frac{\Delta\gamma}{\Delta\lambda}$$

By making $\Delta\lambda$ large, much of the numerical noise can be filtered out, and excellent correspondence between the theory and simulation can be accomplished. Unfortunately, a large $\Delta\lambda$ means that $\Delta\gamma$ is also large. The danger is that γ will change by more than 2π over $\Delta\lambda$, which will cause a large discrepancy between the theory and simulation, since the software is unable to distinguish changes in γ greater than 2π from the equivalent change that is less than 2π. This error can be detected by inspection. When substantial errors occurred in the transmission passband, they were corrected; otherwise, they were ignored.

5.1 Constant transmissivity

Of all the possible transmissivity profiles, constant transmissivity is the easiest to manufacture. The main problem with constant transmissivity is high insertion loss. For the constant coating, the transmission modes are decreasing exponentials. Their asymmetry limits the mode coupling to about 50%, or −3 dB. Combined with the other losses built into the system (window, etalon, and lobe losses that are independent of coating), the maximal theoretical system performance is roughly −4.5 dB. However, since the transmission modes have non-centralized peaks, the bandwidth of constant transmissivity configurations is wide.

TABLE 5-1 summarizes the results of twelve different system configurations with constant transmissivity. These results confirm the expected trends described in SECTION 2 with the exception of unexpected bandwidth reduction at $\Theta = 2.8°$ (see SECTION 6.2). Moreover, the constant dispersion mirror generates very little dispersion deviation over wavelength. Unfortunately, the simpler parabolic mirror suffers from very large deviations over a 0.2 nm range.

Table 5-1: Constant transmissivity scenarios

Θ[a]	Coating[b]	Mirror[c]	Dispersion Bias[d]	σ (ps/nm)[e]	σ_n[f]	Insertion Loss[g]	Bandwidth[h]
2.2°	2.0 %	$r = 3$ cm	-1,725 ps/nm	358	0.2078	-4.91 dB	0.36 nm
2.5°	2.0 %	$r = 3$ cm	-1,419 ps/nm	232	0.1637	-4.61 dB	0.38 nm
2.8°	2.0 %	$r = 3$ cm	-1,289 ps/nm	182	0.1412	-4.50 dB	0.36 nm
2.2°	2.0 %	$K = 70$	-3,161 ps/nm	0.1235	3.907 E-5	-4.96 dB	0.26 nm
2.5°	2.0 %	$K = 70$	-3,161 ps/nm	0.1235	3.907 E-5	-4.71 dB	0.27 nm
2.8°	2.0 %	$K = 70$	-3,161 ps/nm	0.1235	3.907 E-5	-4.62 dB	0.26 nm
2.2°	1.5 %	$r = 3$ cm	-1,342 ps/nm	266	0.1983	-4.79 dB	0.40 nm
2.5°	1.5 %	$r = 3$ cm	-1,165 ps/nm	191	0.1637	-4.55 dB	0.42 nm
2.8°	1.5 %	$r = 3$ cm	-1,061 ps/nm	150	0.1412	-4.45 dB	0.37 nm
2.2°	2.5 %	$r = 3$ cm	-2,037 ps/nm	445	0.2184	-4.96 dB	0.29 nm
2.5°	2.5 %	$r = 3$ cm	-1,690 ps/nm	293	0.1735	-4.69 dB	0.33 nm
2.8°	2.5 %	$r = 3$ cm	-1,424 ps/nm	201	0.1412	-4.56 dB	0.34 nm

a. Incident angle.
b. Power transmissivity of transmissive coating.
c. When r is specified, the mirror is parabolic and r is the radius of curvature. When K is specified, the mirror is a constant dispersion mirror and K is the scaling constant (see SECTION 3.2).
d. Dispersion at the center wavelength defined as the wavelength in the center of the -1 dB band (different from the undeflected wavelength).
e. σ is the standard deviation of the dispersion where $\lambda_k = \lambda_0 + 0.01k$ in nanometers. Note that this computation uses theoretical values.

$$\sigma = \sqrt{\frac{\sum_{k=-10}^{10} (D(\lambda_k) - D(\lambda_0))^2}{21}}$$

f. σ_n is the normalized standard deviation of the dispersion. See above for further explanation

$$\sigma_n^2 = \sqrt{\frac{\sum_{k=-10}^{10} \left(\frac{D(\lambda_k)}{D(\lambda_0)} - 1\right)^2}{21}}$$

g. Insertion loss at the peak wavelength which is not necessarily equal to the center wavelength.
h. -1 dB bandwidth.
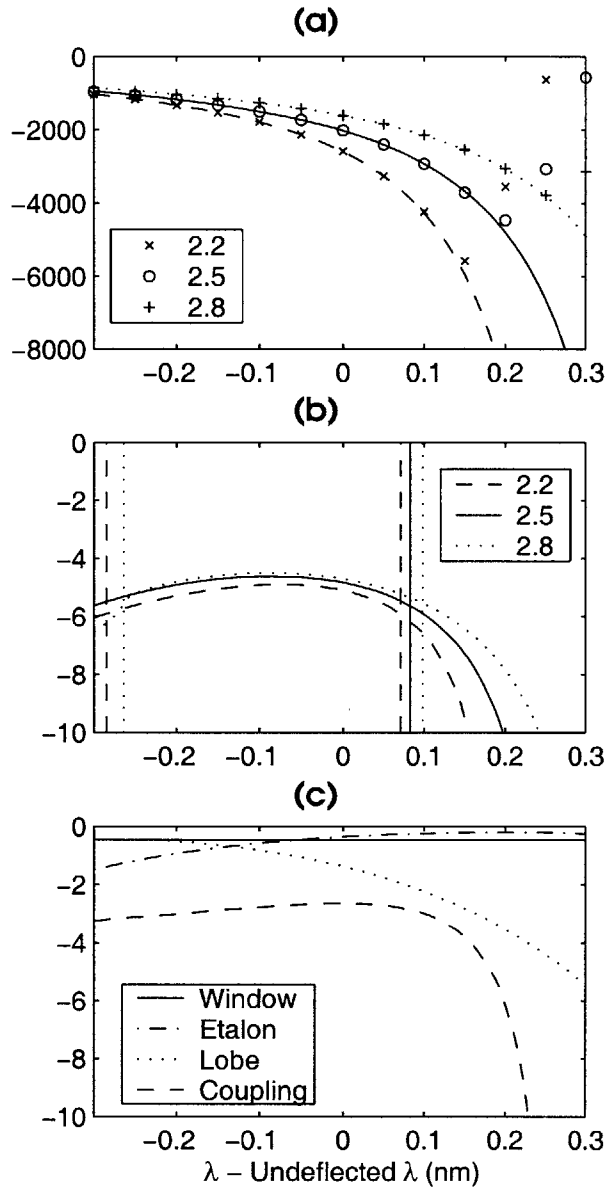
**Figure 5-1: 2.0 % transmissivity,
r = 3 cm parabolic mirror
(Θ = 2.2°, 2.5°, 2.8°).**

(a) Theoretical (lines) and numerical (symbols) dispersion (ps/nm). (b) Transmission spectra and −1 dB band limits (dB). (c) Loss decomposition for Θ = 2.5° (dB).
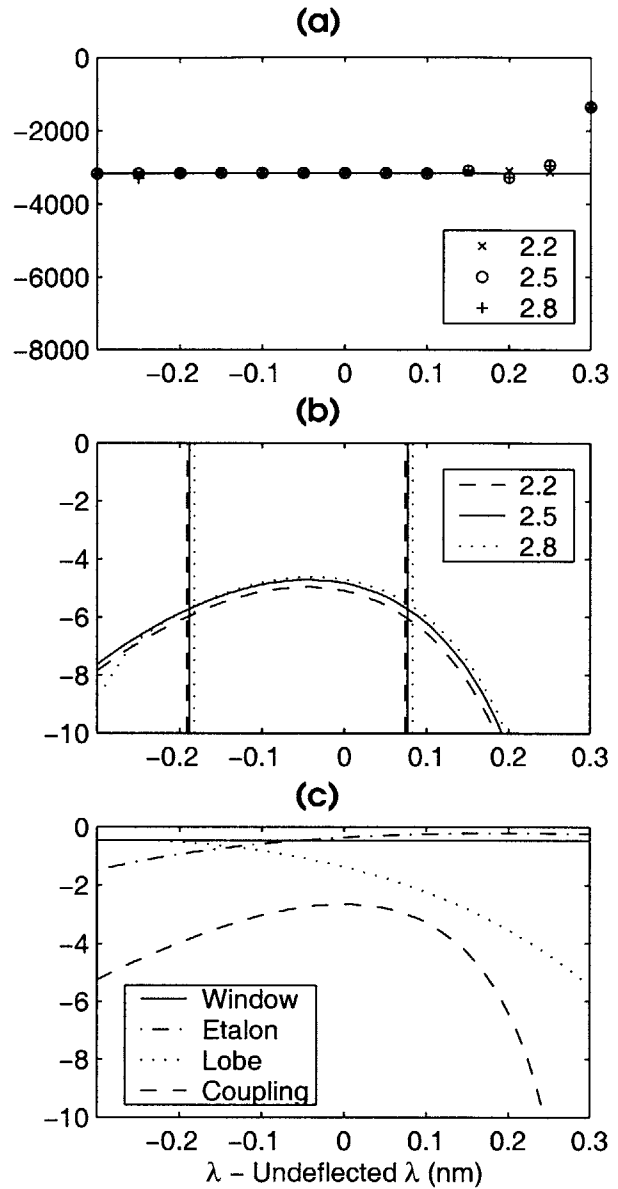
**Figure 5-2: 2.0 % transmissivity,
K = 70 constant dispersion mirror
(Θ = 2.2°, 2.5°, 2.8°).**

(a) Theoretical (lines) and numerical (symbols) dispersion (ps/nm). (b) Transmission spectra and −1 dB band limits (dB). (c) Loss decomposition for Θ = 2.5° (dB).

38
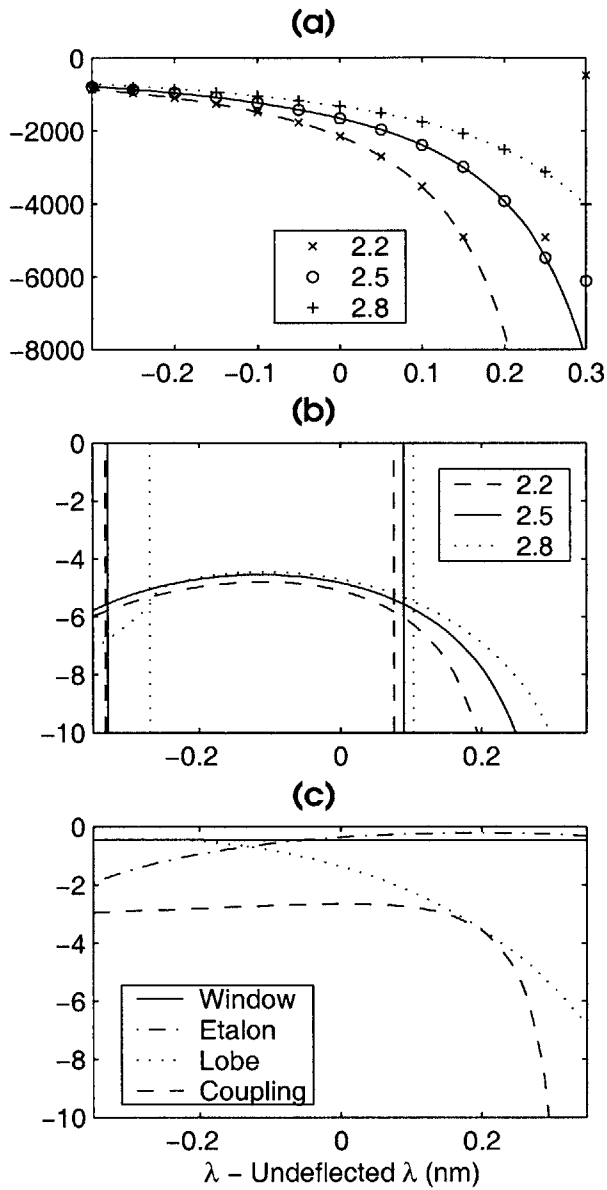
Figure 5-3: 1.5 % transmissivity,
r = 3 cm parabolic mirror
(Θ = 2.2°, 2.5°, 2.8°).

(a) Theoretical (lines) and numerical (symbols) dispersion (ps/nm). (b) Transmission spectra and –1 dB band limits (dB). (c) Loss decomposition for Θ = 2.5° (dB).

Figure 5-4: 2.5 % transmissivity,
r = 3 cm parabolic mirror
(Θ = 2.2°, 2.5°, 2.8°).

(a) Theoretical (lines) and numerical (symbols) dispersion (ps/nm). (b) Transmission spectra and –1 dB band limits (dB). (c) Loss decomposition for Θ = 2.5° (dB).
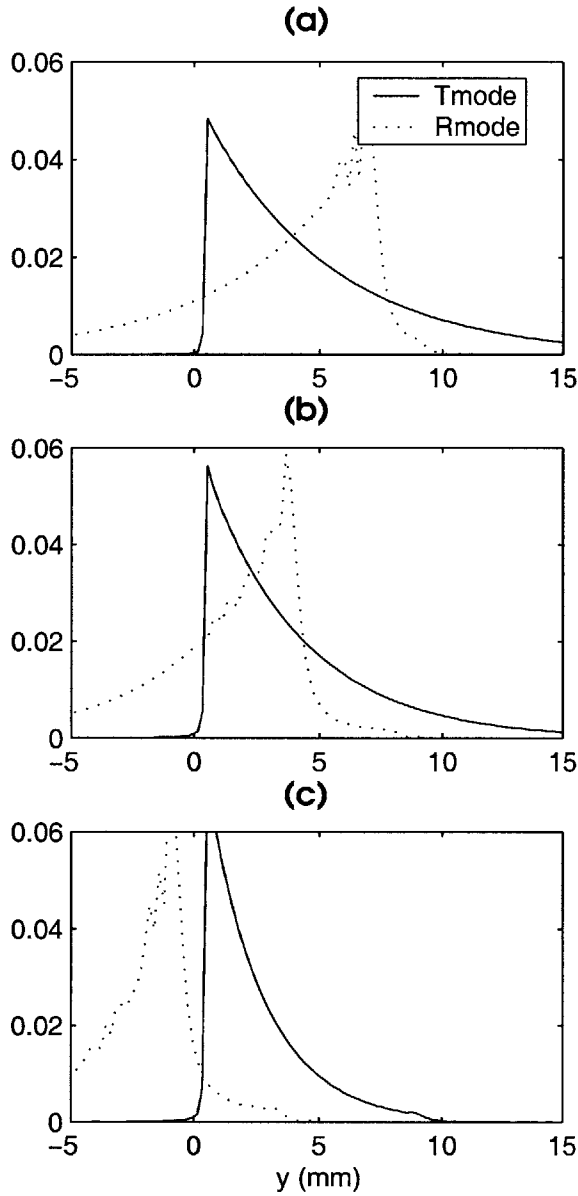
Figure 5-5: 2.0 % transmissivity, r= 3 cm parabolic mirror, transmission and reflection modes at Θ = 2.5° (a.u.).
(a) λ_{ud} - 0.3 nm. (b) λ_{ud}. (c) λ_{ud} + 0.3.
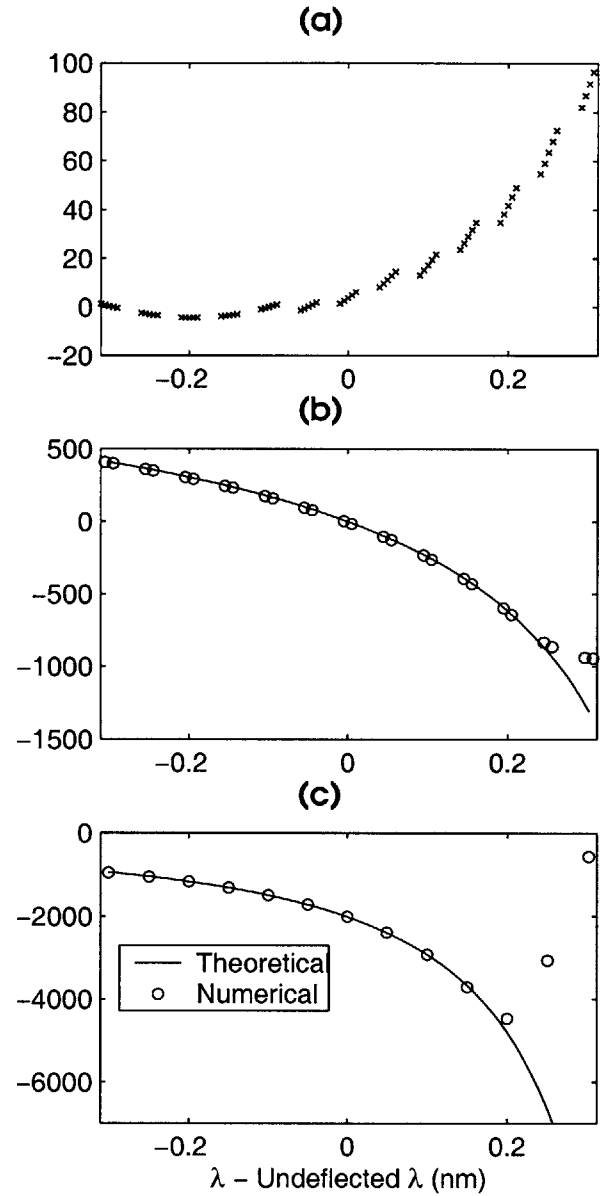
Figure 5-6: 2.0 % transmissivity, r = 3 cm parabolic mirror, dispersion derivation (Θ = 2.5°)
(a) Phase of T_{Mode} and R_{Mode} overlap (γ in radians). (b) Group delay (G = dγ/dω in ps). (c) Dispersion (D = dG/dλ in ps/nm).

---

15. As will be seen in later figures as well, the modes for longer wavelengths are always more narrow than the modes for shorter wavelengths. This is a direct result of the system geometry (see SECTION 6.6).

40

5.2 Linear transmissivity

The only currently observable difference between the linear and constant transmissivity coatings is that the linear coatings have lower insertion loss with nearly 0% coupling loss. This permits a theoretical limit of -2 dB overall insertion loss. Unfortunately, a linear transmissivity coating is difficult to manufacture. Further comparison is performed in SECTION 5.4.

Table 5-2: Linear transmissivity scenarios

Θ	Coating[a]	Mirror	Dispersion Bias	σ (ps/nm)	σ_n	Insertion Loss	Bandwidth
2.2°	40 %/cm	$r = 3$ cm	-879 ps/nm	214	0.2433	-2.40 dB	0.22 nm
2.5°	40 %/cm	$r = 3$ cm	-866 ps/nm	163	0.1885	-2.12 dB	0.25 nm
2.8°	40 %/cm	$r = 3$ cm	-815 ps/nm	123	0.1508	-1.99 dB	0.27 nm
2.2°	40 %/cm	$K = 70$	-3,161 ps/nm	0.1235	3.907 E-5	-2.46 dB	0.13 nm
2.5°	40 %/cm	$K = 70$	-3,161 ps/nm	0.1235	3.907 E-5	-2.20 dB	0.13 nm
2.8°	40 %/cm	$K = 70$	-3,161 ps/nm	0.1235	3.907 E-5	-2.06 dB	0.14 nm
2.5°	20 %/cm	$r = 3$ cm	+144 ps/nm	25	0.1735	-2.01 dB	0.36 nm
2.5°	40 %/cm	$r = 3$ cm	-866 ps/nm	163	0.1885	-2.12 dB	0.25 nm
2.5°	60 %/cm	$r = 3$ cm	-1,358 ps/nm	268	0.1970	-2.17 dB	0.18 nm
2.5°	80 %/cm	$r = 3$ cm	-1,657 ps/nm	334	0.2016	-2.18 dB	0.15 nm
2.5°	10 %/cm	$K = 70$	-3,161 ps/nm	0.1235	3.907 E-5	-2.32 dB	0.21 nm
2.5°	20 %/cm	$K = 70$	-3,161 ps/nm	0.1235	3.907 E-5	-2.16 dB	0.17 nm
2.5°	40 %/cm	$K = 70$	-3,161 ps/nm	0.1235	3.907 E-5	-2.21 dB	0.13 nm
2.5°	60 %/cm	$K = 70$	-3,161 ps/nm	0.1235	3.907 E-5	-2.20 dB	0.11 nm
2.5°	80 %/cm	$K = 70$	-3,161 ps/nm	0.1235	3.907 E-5	-2.20 dB	0.10 nm
2.5°	10 %/cm	$K = 45$	-2,032 ps/nm	0.0794	3.907 E-5	-2.29 dB	0.24 nm
2.5°	20 %/cm	$K = 45$	-2,032 ps/nm	0.0794	3.907 E-5	-2.15 dB	0.21 nm
2.5°	40 %/cm	$K = 45$	-2,032 ps/nm	0.0794	3.907 E-5	-2.17 dB	0.17 nm
2.5°	60 %/cm	$K = 45$	-2,032 ps/nm	0.0794	3.907 E-5	-2.18 dB	0.15 nm
2.5°	80 %/cm	$K = 45$	-2,032 ps/nm	0.0794	3.907 E-5	-2.19 dB	0.13 nm

a. Amplitude transmissivity.
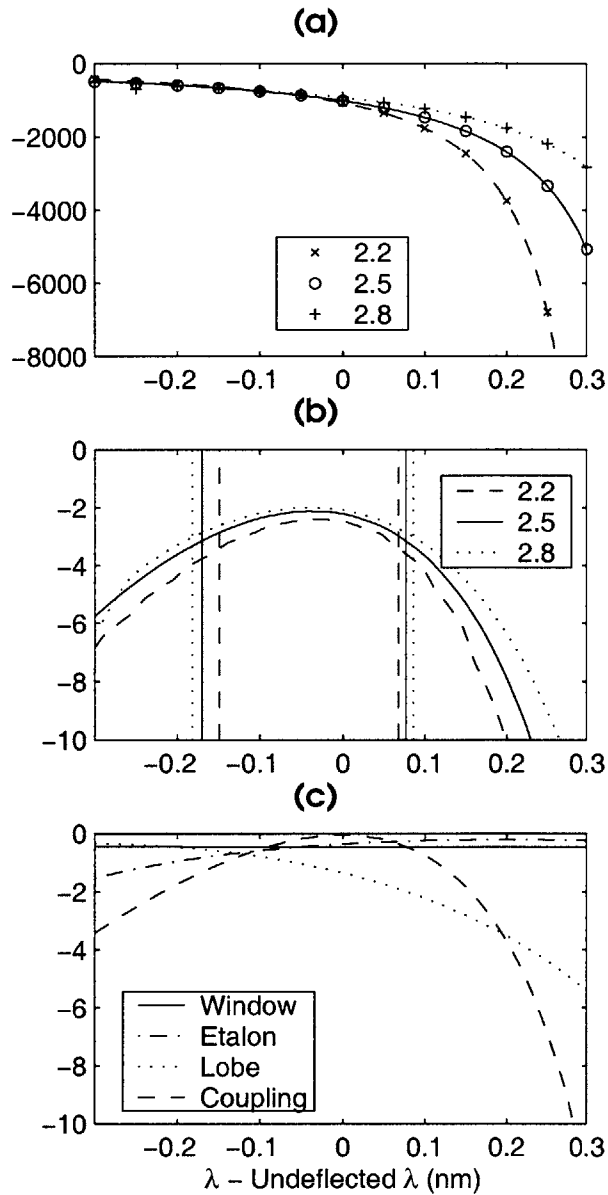
Figure 5-7: 40%/cm transmissivity, r = 3 cm parabolic mirror (Θ = 2.2°, 2.5°, 2.8°).
(a) Theoretical (lines) and numerical (symbols) dispersion (ps/nm). (b) Transmission spectra and −1 dB band limits (dB). (c) Loss decomposition for Θ = 2.5° (dB).

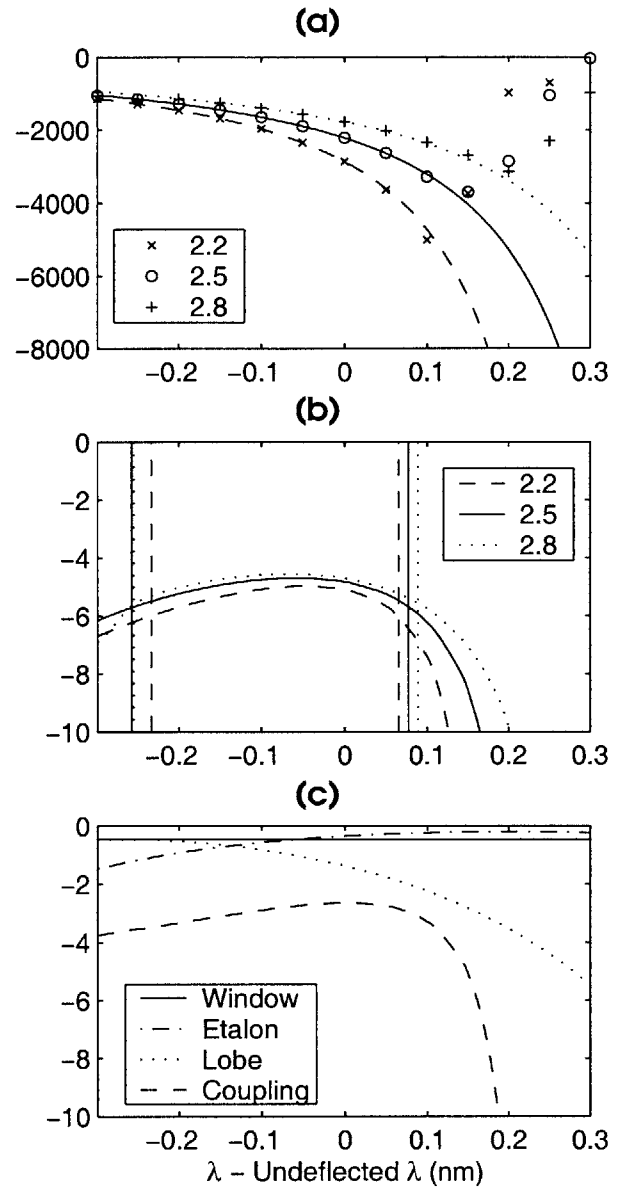**Figure 5-8: 40%/cm transmissivity, K = 70 constant dispersion mirror (Θ = 2.2°, 2.5°, 2.8°).**
(a) Theoretical (lines) and numerical (symbols) dispersion (ps/nm). (b) Transmission spectra and −1 dB band limits (dB). (c) Loss decomposition for Θ = 2.5° (dB).

Figure 5-9: Varied linear transmissivity, r = 3 cm parabolic mirror (slope = 40, 60, 80 %/cm, Θ = 2.5°). (a) Theoretical (lines) and numerical (symbols) dispersion (ps/nm). (b) Transmission spectra and −1 dB band limits (dB). (c) Loss decomposition for slope = 60 %/cm (dB).

Figure 5-10: Varied linear transmissivity, K = 70 & 45 constant dispersion mirrors (slope = 10, 20, 40 %/cm, Θ = 2.5°). (a) Theoretical (lines) and numerical (symbols) dispersion (ps/nm). (b) Trans. spectra and −1 dB limits (K = 70) (dB). (c) Trans. spectra and -1 dB limits (K = 45) (dB).
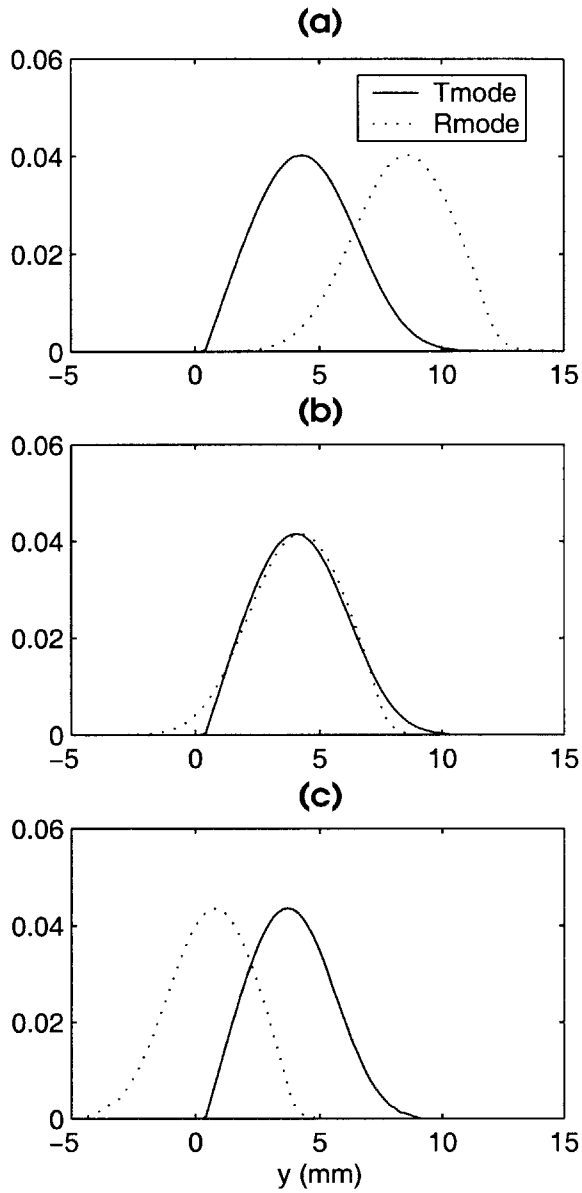
Figure 5-11: 40%/cm transmissivity, K = 70 constant dispersion mirror, transmission and reflection modes at Θ = 2.5° (a.u.).
(a) λ_{ud} - 0.3 nm. (b) λ_{ud}. (c) λ_{ud} + 0.3.
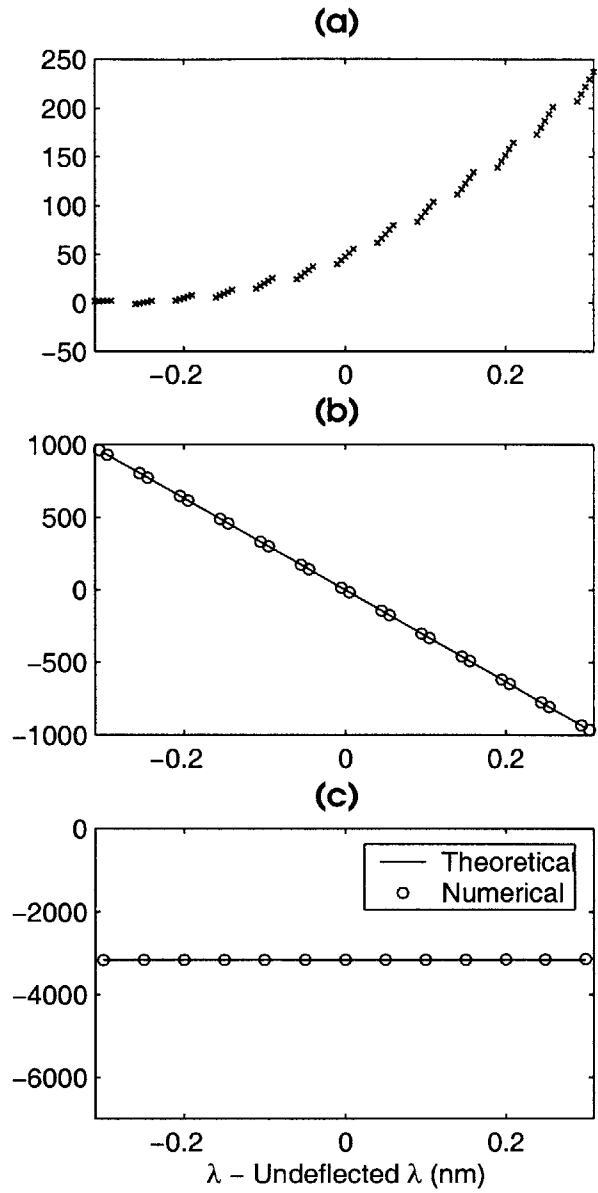
Figure 5-12: 40%/cm transmissivity, K = 70 constant dispersion mirror, dispersion derivation (Θ = 2.5°).
(a) Phase of T_{Main} and R_{Main} overlap (γ in radians). (b) Group delay (G = dγ/dω in ps). (c) Dispersion (D = dG/dλ in ps/nm).

5.3 Multi-level transmissivity

The multi-level transmissivity is an approximation of the linear transmissivity case that is easier to manufacture. However, the levels do not approximate the linear amplitude transmissivity of the linear case templates; they approximate the parabolic power transmissivity. Intuitively, this is because the performance of the compensator is measured with respect to power, and therefore the power response should be approximated. For the following 2-level cases, the junction is located at roughly 1/2 of the linear
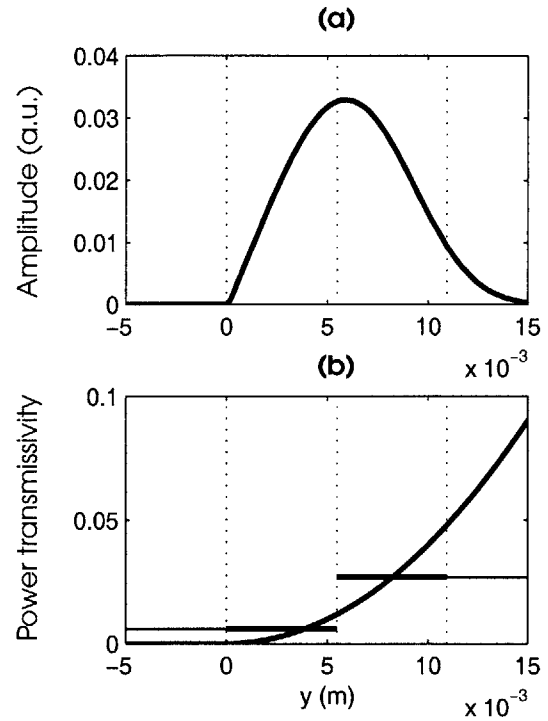
Figure 5-13: 2-level transmissivity determination
(a) Linear template T_{Mode}.
(b) 2-level profile with window at y = 0.

template undeflected wavelength transmission mode width, and the power transmissivity levels are the arithmetic means of the parabolic endpoints of each region (see FIGURE 5-13).[16] The same method is repeated for the 3-level cases, except that the linear template undeflected wavelength transmission mode width is divided into thirds. The main distinction of the multi-level cases is that the insertion loss hovers around −3.0 dB. For the 3-level cases, the transmission spectra can be designed to have a dip in the middle. This would increase the effective bandwidth of the VIPA compensator cascaded with a device that has a more typical transmission spectrum with a peak in the center.

---

16. This level determination algorithm only provides an initial guess for good designs. By exploring the junction-level combinations in the neighborhood of this guess, low insertion loss and wide bandwidth configurations can be found.

Table 5-3: 2-level transmissivity scenarios

Θ	Template	Mirror	Dispersion Bias	σ (ps/nm)	σ_n	Insertion Loss	Bandwidth
2.5°	40 %/cm	$r = 3$ cm	-1,213 ps/nm	207	0.1701	-2.97 dB	0.32 nm
2.5°	60 %/cm	$r = 3$ cm	-1,573 ps/nm	284	0.1806	-3.12 dB	0.27 nm
2.5°	80 %/cm	$r = 3$ cm	-1,773 ps/nm	327	0.1845	-3.10 dB	0.22 nm
2.5°	10 %/cm	$K = 70$	-3,161 ps/nm	0.1235	3.907 E-5	-2.97 dB	0.30 nm
2.5°	20 %/cm	$K = 70$	-3,161 ps/nm	0.1235	3.907 E-5	-3.00 dB	0.26 nm
2.5°	40 %/cm	$K = 70$	-3,161 ps/nm	0.1235	3.907 E-5	-3.01 dB	0.18 nm
2.5°	10 %/cm	$K = 45$	-2,032 ps/nm	0.0794	3.907 E-5	-2.95 dB	0.36 nm
2.5°	20 %/cm	$K = 45$	-2,032 ps/nm	0.0794	3.907 E-5	-2.97 dB	0.33 nm
2.5°	40 %/cm	$K = 45$	-2,032 ps/nm	0.0794	3.907 E-5	-3.00 dB	0.25 nm

Table 5-4: Level values and junction location for 2-level transmissivity

T_0^2	J_1	T_1^2
0.98 %	0.35 cm	4.90 %
1.12 %	0.25 cm	5.63 %
1.28 %	0.20 cm	6.40 %
0.32 %	0.80 cm	1.60 %
0.60 %	0.55 cm	3.02 %
0.98 %	0.35 cm	4.90 %
0.32 %	0.80 cm	1.60 %
0.60 %	0.55 cm	3.02 %
0.98 %	0.35 cm	4.90 %
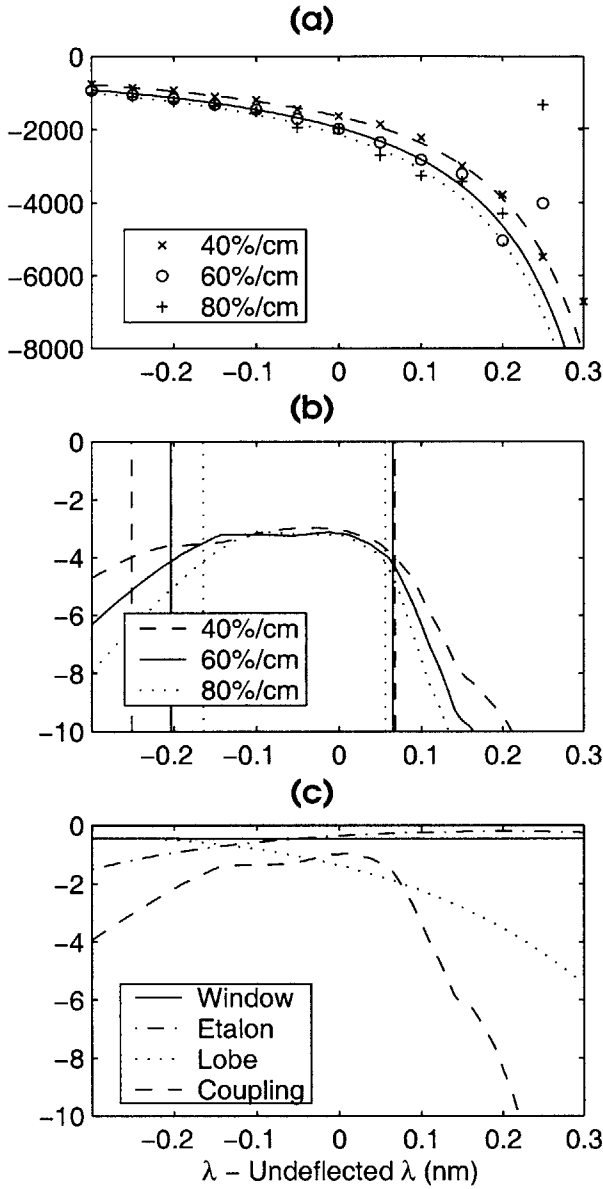
Figure 5-14: 2-level transmissivity, r = 3 cm parabolic mirror (template = 40, 60, 80 %/cm).
(a) Theoretical (lines) and numerical (symbols) dispersion (ps/nm). (b) Transmission spectra and –1 dB band limits (dB). (c) Loss decomposition for slope = 60 %/cm (dB).

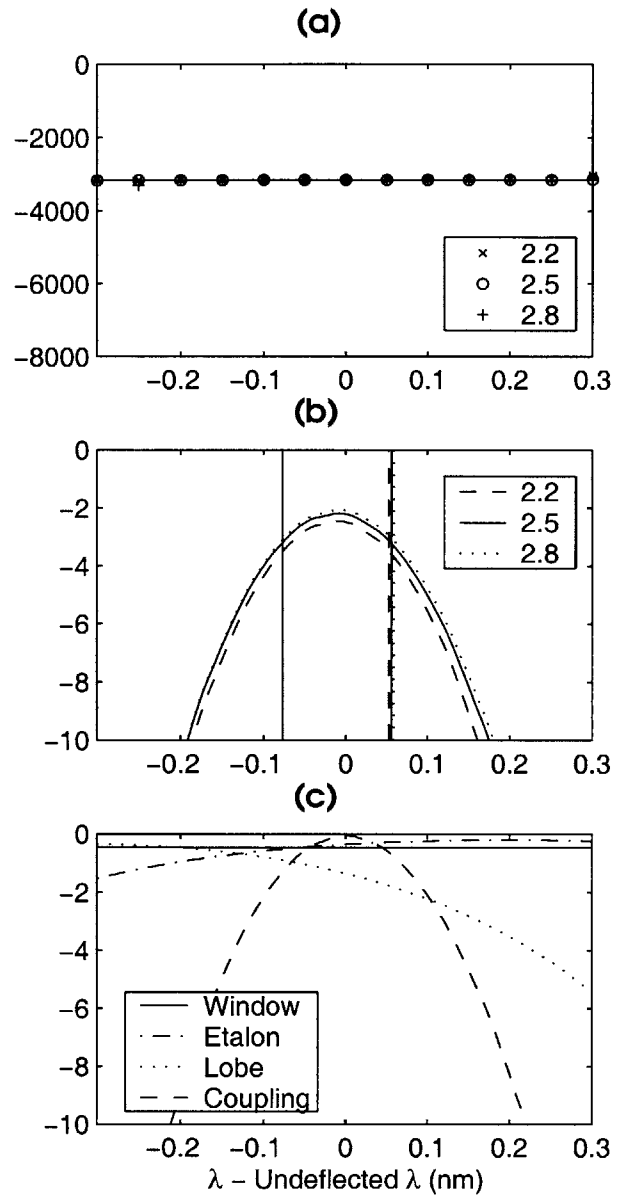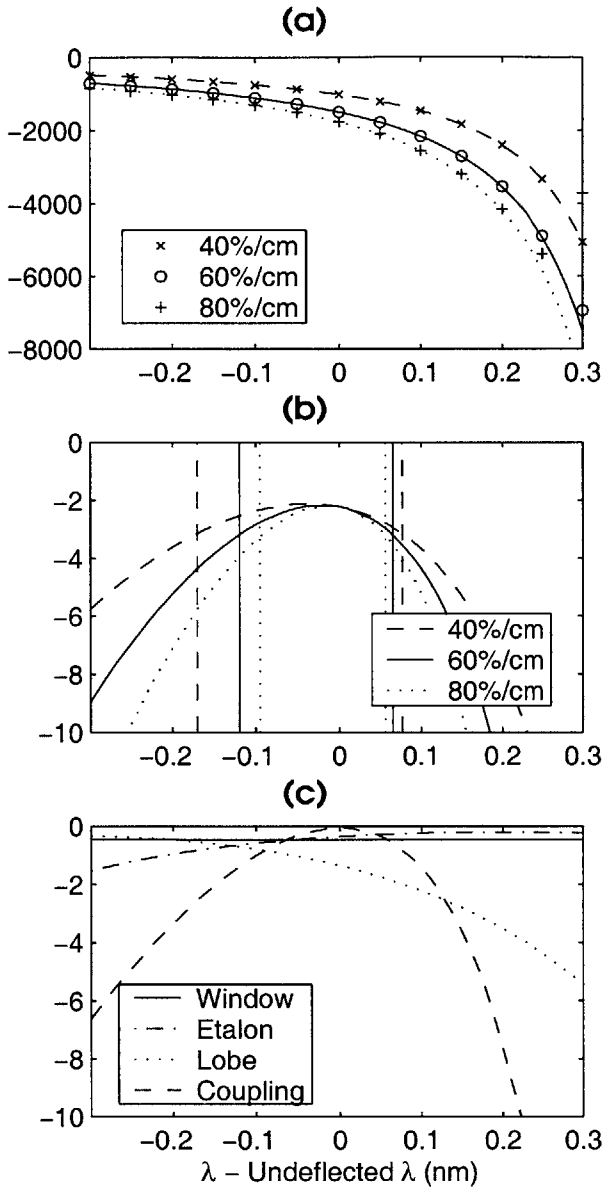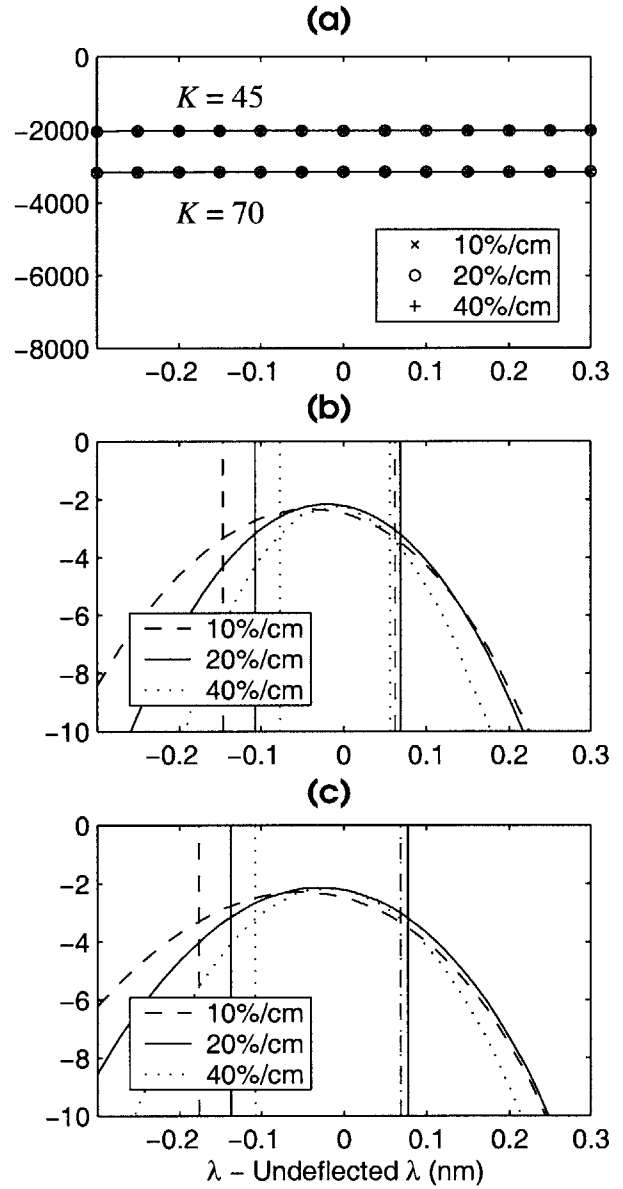**Figure 5-15: 2-level transmissivity, K = 70 constant dispersion mirror (template = 10, 20, 40 %/cm).**
(a) Theoretical (lines) and numerical (symbols) dispersion (ps/nm). (b) Transmission spectra and –1 dB band limits (dB). (c) Loss decomposition for slope = 20 %/cm (dB).

(a)

(b)

(c)

λ – Undeflected λ (nm)

(a)

(b)

(c)

y (mm)

Figure 5-16: 2-level transmissivity, K = 45 constant dispersion mirror (template = 10, 20, 40 %/cm).
(a) Theoretical (lines) and numerical (symbols) dispersion (ps/nm). **(b)** Transmission spectra and –1 dB band limits (dB). **(c)** Loss decomposition for slope = 20 %/cm (dB).

Figure 5-17: 20%/cm 2-level trans., K = 70 constant dispersion mirror, transmission and reflection modes, at Θ = 2.5° (a.u.).
(a) λ_{ud} - 0.3 nm. **(b)** λ_{ud}. **(c)** λ_{ud} + 0.3.

48

Table 5-5: 3-level transmissivity scenarios

Θ	Template	Mirror	Dispersion Bias	σ (ps/nm)	σ_n	Insertion Loss	Bandwidth
2.5°	40 %/cm	$r = 3$ cm	-1,203 ps/nm	205	0.1701	-3.00 dB	0.34 nm
2.5°	60 %/cm	$r = 3$ cm	-1,573 ps/nm	284	0.1806	-3.03 dB	0.26 nm
2.5°	80 %/cm	$r = 3$ cm	-1,796 ps/nm	354	0.1970	-2.53 dB	0.14 nm
2.5°	10 %/cm	$K = 70$	-3,161 ps/nm	0.1235	3.907 E-5	-2.90 dB	0.24 nm
2.5°	20 %/cm	$K = 70$	-3,161 ps/nm	0.1235	3.907 E-5	-3.17 dB	0.21 nm
2.5°	40 %/cm	$K = 70$	-3,161 ps/nm	0.1235	3.907 E-5	-3.10 dB	0.20 nm
2.5°	10 %/cm	$K = 45$	-2,032 ps/nm	0.0794	3.907 E-5	-2.87 dB	0.29 nm
2.5°	20 %/cm	$K = 45$	-2,032 ps/nm	0.0784	3.907 E-5	-3.16 dB	0.24 nm
2.5°	40 %/cm	$K = 45$	-2,032 ps/nm	0.0784	3.907 E-5	-3.06 dB	0.27 nm

Table 5-6: Level values and junction locations for 3-level transmissivity

T_0^2	J_1	T_1^2	J_2	T_2^2
0.89 %	0.33 cm	4.44 %	0.67 cm	11.56 %
1.125 %	0.25 cm	5.625 %	0.50 cm	14.625 %
8.889 %	0.17 cm	4.444 %	0.33 cm	11.56 %
0.22 %	0.67 cm	1.11 %	1.33 cm	2.89 %
0.50 %	0.50 cm	2.50 %	1.00 cm	6.50 %
0.89 %	0.33 cm	4.44 %	0.67 cm	11.56 %
0.22 %	0.67 cm	1.11 %	1.33 cm	2.89 %
0.50 %	0.50 cm	2.50 %	1.00 cm	6.50 %
0.89 %	0.33 cm	4.44 %	0.67 cm	11.56 %
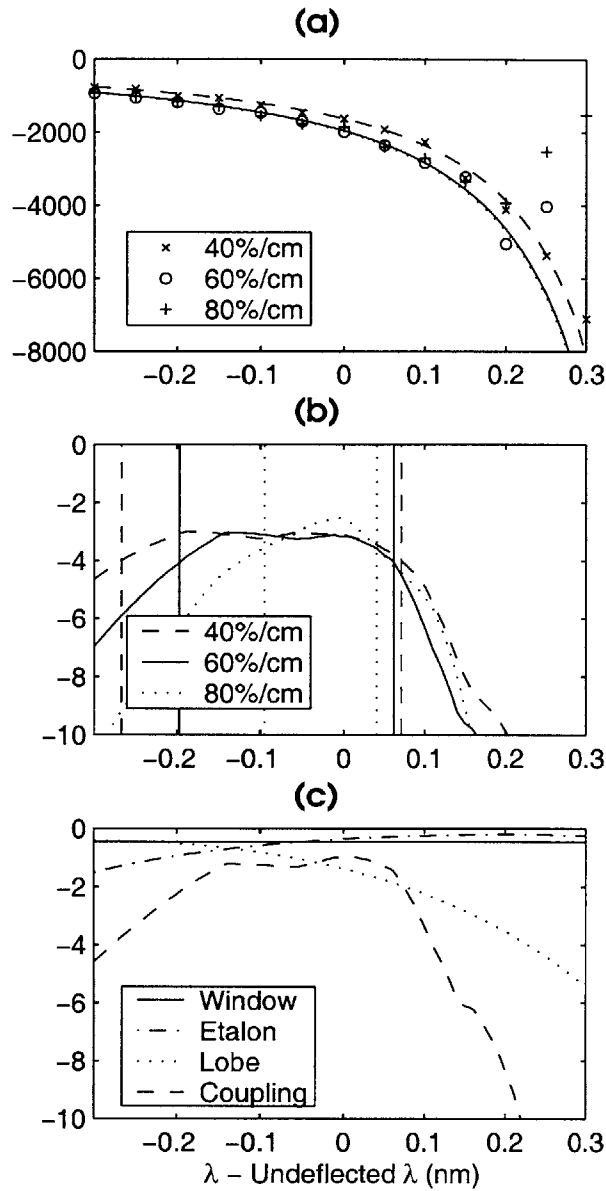
**Figure 5-18: 3-level transmissivity,
r = 3 cm parabolic mirror
(template = 40, 60, 80 %/cm).**
(a) Theoretical (lines) and numerical (symbols) dispersion (ps/nm). (b) Transmission spectra and –1 dB band limits (dB). (c) Loss decomposition for slope = 60 %/cm (dB).
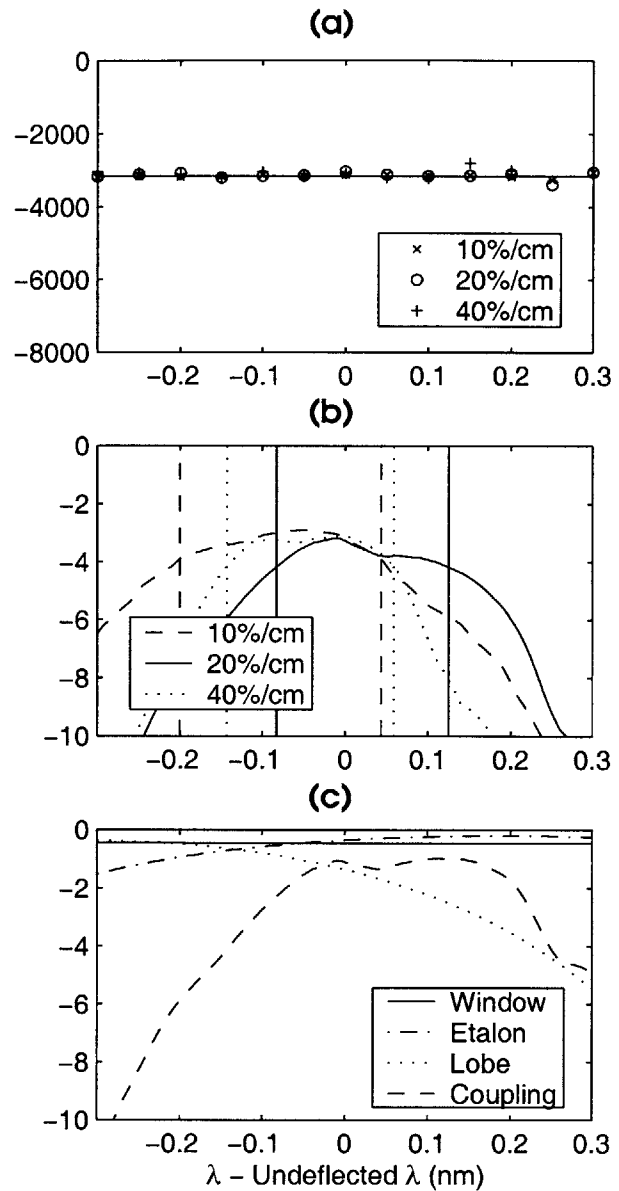
**Figure 5-19: 3-level transmissivity,
K = 70 constant dispersion mirror
(template = 10, 20, 40 %/cm).**
(a) Theoretical (lines) and numerical (symbols) dispersion (ps/nm). (b) Transmission spectra and –1 dB band limits (dB). (c) Loss decomposition for slope = 20 %/cm (dB).

(a)

×	10%/cm
o	20%/cm
+	40%/cm

(a)

— Tmode
⋯ Rmode

(b)

– –	10%/cm
——	20%/cm
⋯	40%/cm

(b)

(c)

——	Window
– –	Etalon
⋯	Lobe
– –	Coupling

λ – Undeflected λ (nm)

(c)

y (mm)
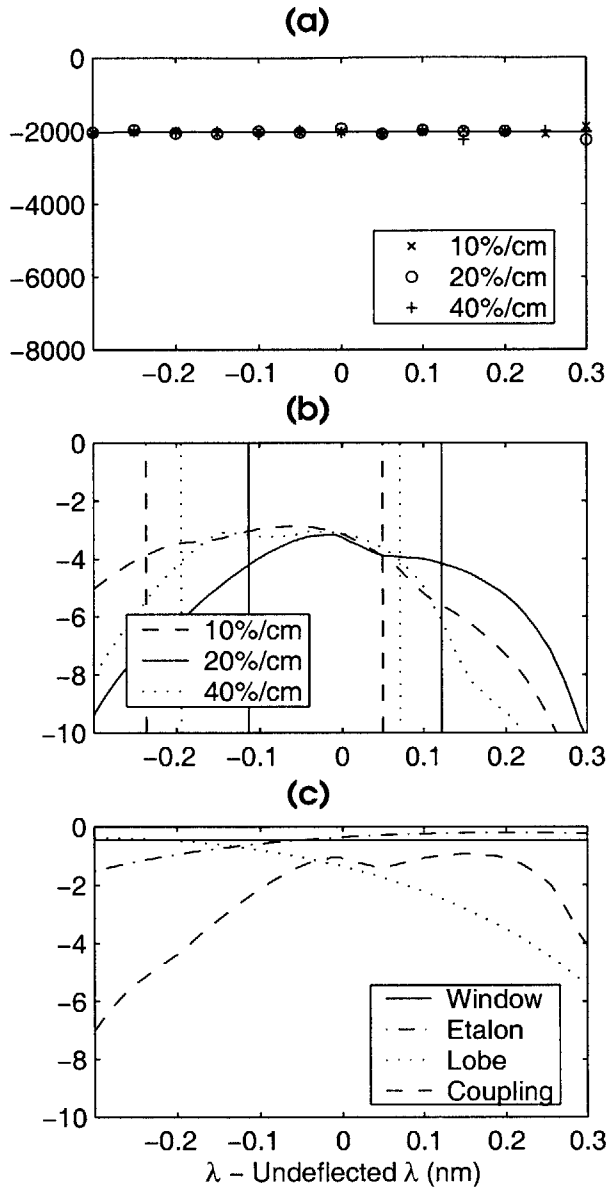
Figure 5-20: 3-level transmissivity, K = 45 constant dispersion mirror (template = 10, 20, 40 %/cm).
(a) Theoretical (lines) and numerical (symbols) dispersion (ps/nm). (b) Transmission spectra and –1 dB band limits (dB). (c) Loss decomposition for slope = 20 %/cm (dB).

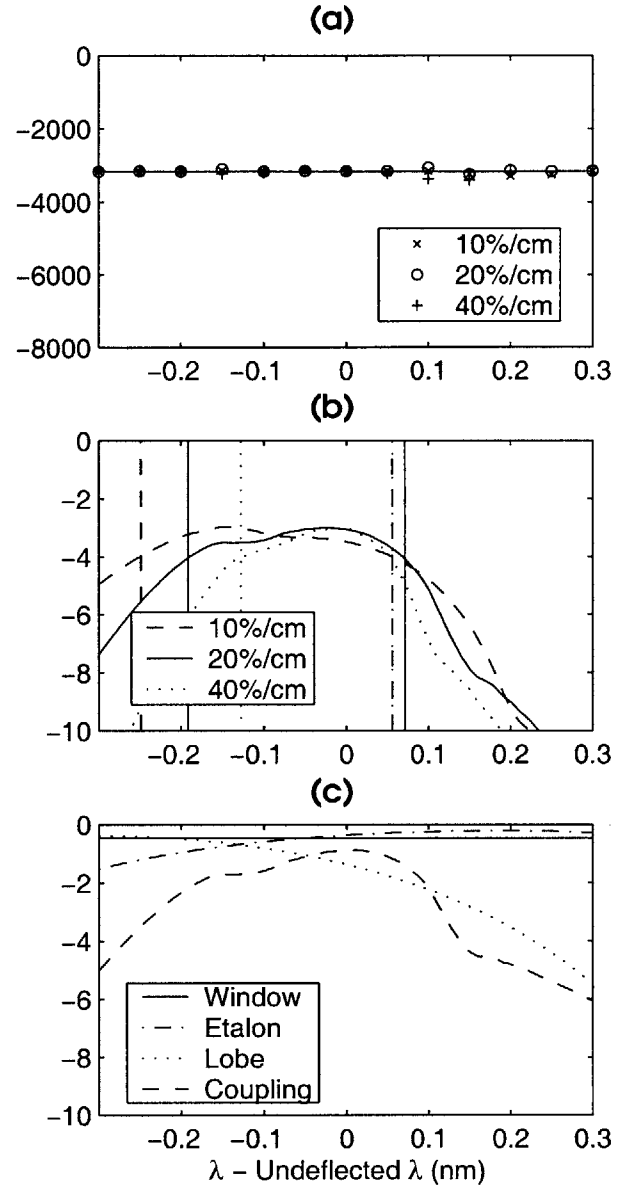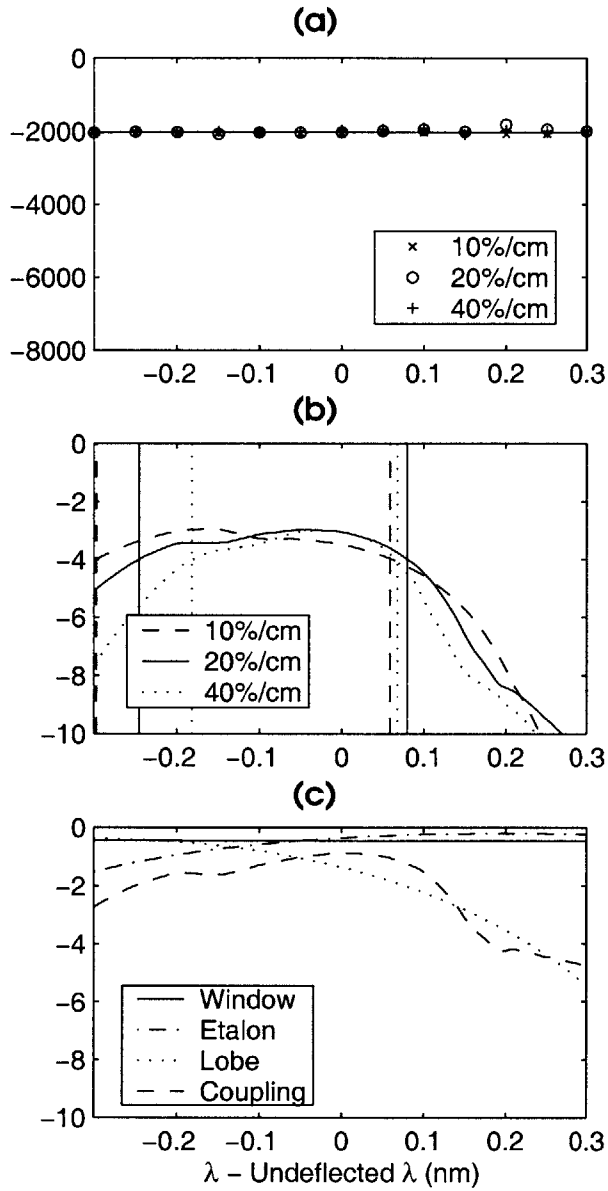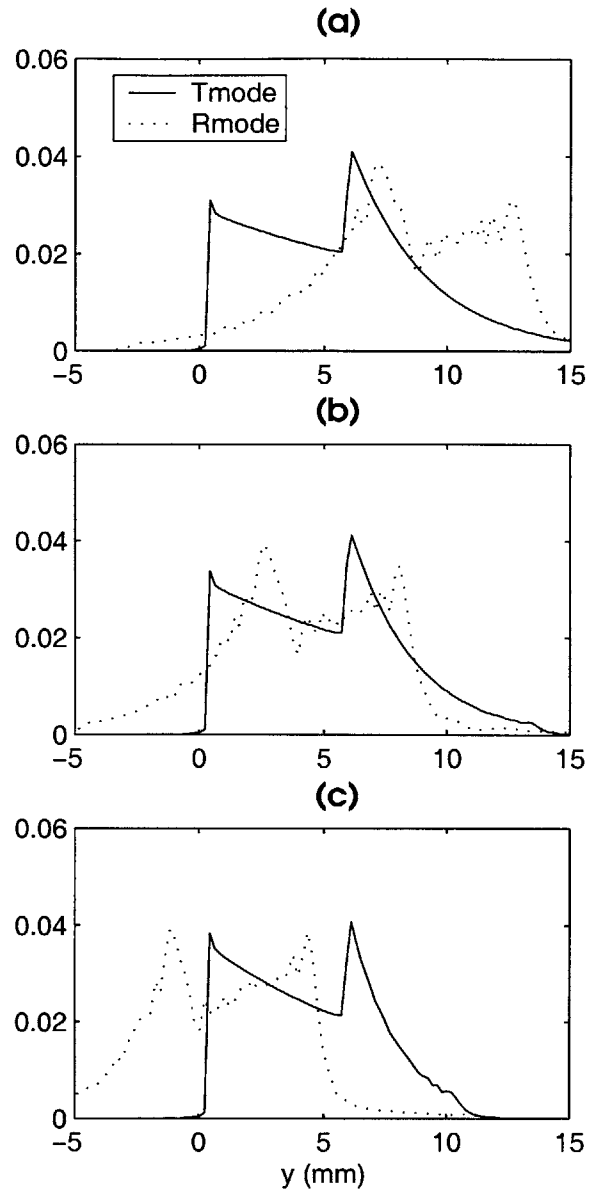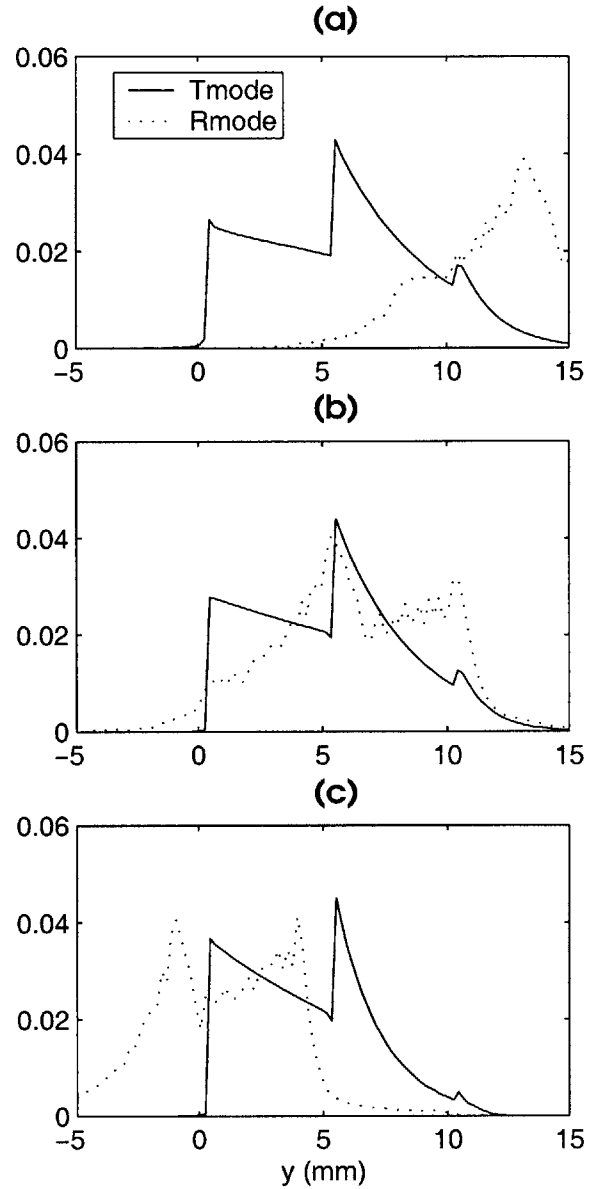**Figure 5-21: 20%/cm 3-level trans., K = 70 constant dispersion mirror, transmission and reflection modes at $\Theta = 2.5°$ (a.u.).**
(a) λ_{ud} - 0.3 nm. (b) λ_{ud}. (c) λ_{ud} + 0.3.

51

5.4 Constrained coating comparison

These three coating designs must be constrained in order to be meaningfully compared. The two constraints in this exercise are that they produce the same dispersion (using a constant dispersion mirror) and that their transmission mode widths be the same. The transmission mode widths should be the same so that all three configurations can use an etalon of the same size. FIGURE 5-22 shows the transmission and reflection modes for the undeflected wavelength as well as the transmission spectra and −1 dB bands for the three cases.
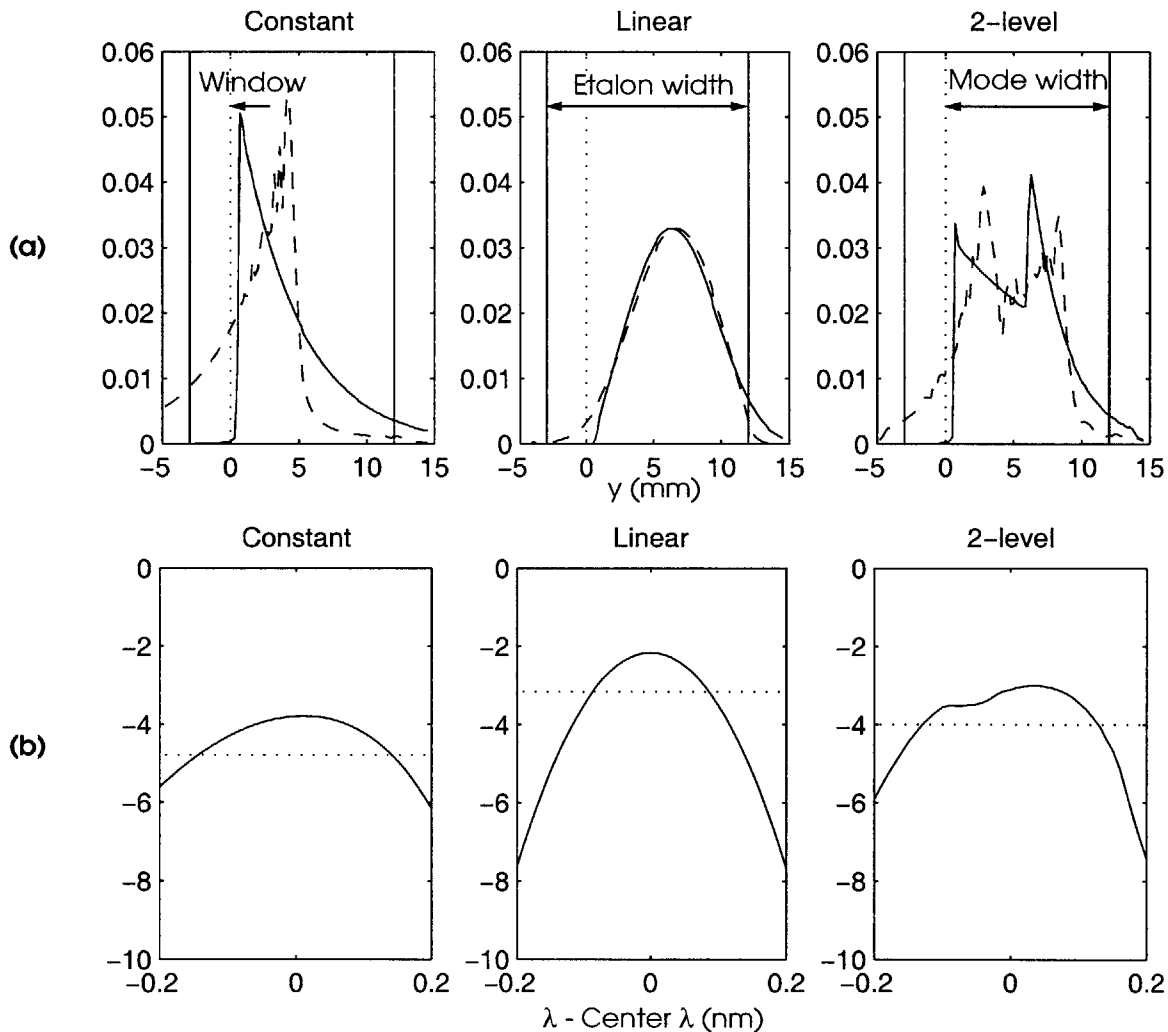
Figure 5-22: Constrained coating comparison
(a) Transmission and reflection modes at undeflected wavelength
(b) Transmission spectra and −1dB bands

TABLE 5-7 summarizes the simulation results. The constant case has wide bandwidth, but suffers from high insertion loss. The linear case exhibits low insertion loss, but has narrow bandwidth. The 2-level case is superior to both, since it has low insertion loss and wide bandwidth.

Table 5-7: Constrained coating comparison

Coating	Insertion loss	Bandwidth	Dispersion
Constant power (1.8%)	-4.7 dB	0.29 nm	-3,200 ps/nm
Linear amplitude (20%/cm)	-2.2 dB	0.17 nm	-3,200 ps/nm
2-level (20%/cm template)	-3.0 dB	0.26 nm	-3,200 ps/nm

To put these numbers in context, -3,200 ps/nm is enough dispersion to compensate 200 km of standard single mode fiber. The same task would require on the order of 50 km of DCF. The transmission spectrum of DCF is flat over a single WDM channel but the insertion loss would be in the vicinity of -20 dB. Even the constant coating is better in this respect by a wide margin.

The fundamental reason for the VIPA compensator's superiority is that its insertion loss is independent of dispersion. The preceding tables (TABLES 5-1, 5-2, 5-3, and 5-5) show that insertion loss depends only on coating type. Insertion loss is related to bandwidth insofar as coating type influences bandwidth, but there is no direct relationship between bandwidth and insertion loss. The system trade-off is between bandwidth and dispersion. The bandwidth decreases as dispersion increases, but insertion loss stays fixed. Since insertion loss is independent of dispersion, using a VIPA compensator can reduce the number of optical amplifiers needed along a communications link.

5.5 Tunable compensator

The VIPA compensator can be tuned over a range of as much as 1,500 ps/nm by varying

the distance l between the etalon and the lens by as little as 10 cm. This varies the parameter a that

appears in the dispersion formula.

Table 5-8: Tunable compensator (r = 3 cm)

l (cm)	Θ	Coating	Mirror	Dispersion Bias	σ (ps/nm)	σ_n	Insertion Loss	Bandwidth
0.5	2.5°	2.0 %	$r = 3$ cm	-1,419 ps/nm	232	0.1637	-4.61 dB	0.38 nm
1.0	2.5°	2.0 %	$r = 3$ cm	-1,336 ps/nm	219	0.1637	-4.60 dB	0.39 nm
2.0	2.5°	2.0 %	$r = 3$ cm	-1,169 ps/nm	191	0.1637	-4.58 dB	0.40 nm
3.0	2.5°	2.0 %	$r = 3$ cm	-1,001 ps/nm	164	0.1637	-4.55 dB	0.41 nm
4.0	2.5°	2.0 %	$r = 3$ cm	-813 ps/nm	131	0.1607	-4.53 dB	0.42 nm
5.0	2.5°	2.0 %	$r = 3$ cm	-650 ps/nm	105	0.1607	-4.51 dB	0.43 nm
6.0	2.5°	2.0 %	$r = 3$ cm	-488 ps/nm	78	0.1607	-4.50 dB	0.43 nm
7.0	2.5°	2.0 %	$r = 3$ cm	-325 ps/nm	52	0.1607	-4.48 dB	0.44 nm
8.0	2.5°	2.0 %	$r = 3$ cm	-158 ps/nm	25	0.1578	-4.47 dB	0.44 nm
9.0	2.5°	2.0 %	$r = 3$ cm	+0.93 ps/nm	0.1465	0.1578	-4.47 dB	0.44 nm
10.0	2.5°	2.0 %	$r = 3$ cm	+160 ps/nm	25	0.1578	-4.47 dB	0.44 nm
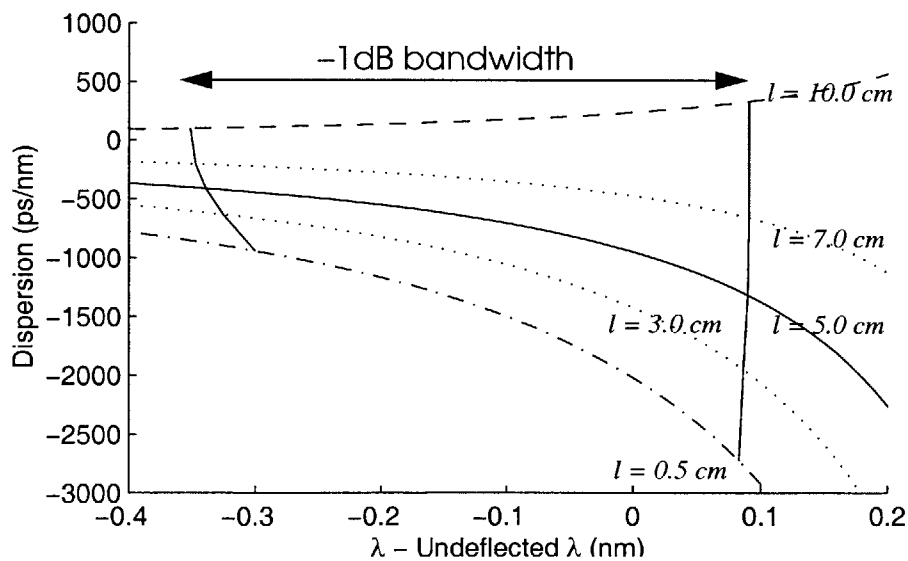
Figure 5-23: Tunable dispersion variation for parabolic mirror

54

The parabolic mirror's σ_n stays large but constant over the tuning range. The constant dispersion mirror's σ_n increases towards the tuning range extremities. In both cases, insertion loss and bandwidth remain fairly constant.

Table 5-9: Tunable compensator (K = 30)[a]

l (cm)	Θ	Coating	Mirror	Dispersion Bias	σ (ps/nm)	σ_n	Insertion Loss	Bandwidth
1.0	2.5°	2.0 %	$K = 30$	-2,079 ps/nm	126	0.0604	-4.65 dB	0.34 nm
2.0	2.5°	2.0 %	$K = 30$	-1,898 ps/nm	94	0.0496	-4.64 dB	0.35 nm
3.0	2.5°	2.0 %	$K = 30$	-1,707 ps/nm	60	0.0351	-4.61 dB	0.37 nm
4.0	2.5°	2.0 %	$K = 30$	-1,531 ps/nm	30	0.0196	-4.59 dB	0.38 nm
5.0	2.5°	2.0 %	$K = 30$	-1,355 ps/nm	0.0529	3.907 E-5	-4.57 dB	0.39 nm
6.0	2.5°	2.0 %	$K = 30$	-1,183 ps/nm	29	0.0242	-4.55 dB	0.40 nm
7.0	2.5°	2.0 %	$K = 30$	-1,021 ps/nm	55	0.0536	-4.53 dB	0.41 nm
8.0	2.5°	2.0 %	$K = 30$	-853 ps/nm	82	0.0962	-4.51 dB	0.42 nm
9.0	2.5°	2.0 %	$K = 30$	-683 ps/nm	109	0.1595	-4.49 dB	0.43 nm
10.0	2.5°	2.0 %	$K = 30$	-541 ps/nm	131	0.2421	-4.48 dB	0.43 nm

a. Mirror optimized for $l = 5.0$ cm.
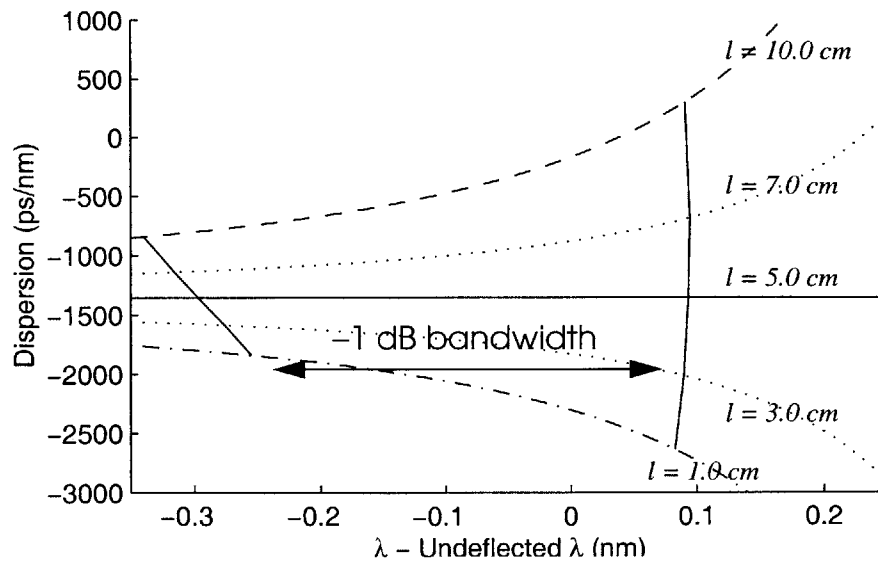
Figure 5-24: Tunable dispersion variation for constant dispersion mirror

6.0 Finer Points

This section describes some of the more subtle and practical considerations regarding the design of a VIPA compensator.

6.1 Predicting center wavelength

All of the simulation results presented in the previous section were designed so that Φ for the undeflected wavelength $\lambda = 1550$ nm was equal to Θ. The focusing lens was aligned to minimize coupling loss at that same wavelength as well.[17] Unfortunately, the lobe loss is not, in general, minimized at $\Phi = \Theta$; it is minimized when $\Phi > \Theta$, which corresponds to $\lambda < \lambda_{1550}$. This is because the light bouncing back and forth between the etalon surfaces rapidly loses its Gaussian shape, so that the virtual image approximation is not quite valid (see FIGURE 4-1). This deviation from the ideal is responsible for the shift between the wavelength with the least lobe loss and the undeflected wavelength.

The VIPA idealization for the constant coating assumes an array of in phase Gaussian beams of decreasing magnitude offset by $2t$ and propagating at Θ (see FIGURE 6-1).
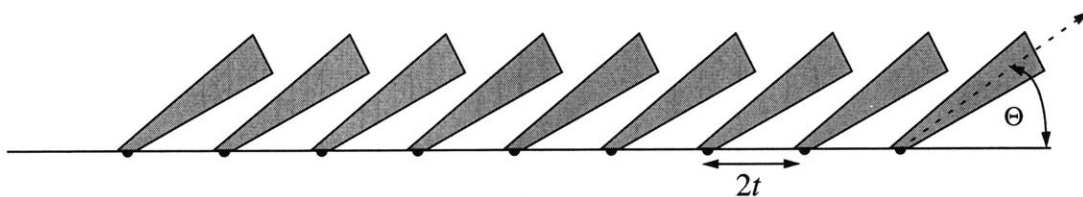
Figure 6-1: VIPA Gaussian beam idealization

---

17. The thickness of the plate, t, was fine-tuned so that Φ (λ=1550 nm) was always equal to Θ (see EQUATION 2.1). The coupling loss minimization at $\lambda = 1550$ nm is accomplished by tilting the lens $-\Theta$ with respect to the etalon (so that the light at 1550 nm is normally incident on the lens) and aligning the lens axis with the power center of the main 1550 nm transmission mode (see SECTION 4.3).

The far-field pattern or, equivalently, the pattern in the focusing-lens focal plane is:

$$V_{Ideal} = \exp\left(\frac{-w_o^2(k_y - k_0)^2}{4}\right) \sum_{p=0}^{\infty} \alpha^p \exp\left(j2tk_n p\left(1 - \frac{1}{2}\left(\frac{k_y}{k_n}\right)^2\right)\right)$$

$$k_0 = k_n \sin\theta$$

$$V_{Ideal} = \frac{\exp\left(\frac{-w_o^2(k_y - k_0)^2}{4}\right)}{1 - \alpha\exp\left(j2tk_n\left(1 - \frac{1}{2}\left(\frac{k_y}{k_n}\right)^2\right)\right)}$$

$$|V_{Ideal}|^2 = \frac{\exp\left(\frac{-w_o^2(k_y - k_0)^2}{4}\right)^2}{1 + \alpha^2 - 2\alpha\cos\left(2tk_n\left(1 - \frac{1}{2}\left(\frac{k_y}{k_n}\right)^2\right)\right)}$$

The intensity expression can be divided into an envelope and a modulation:
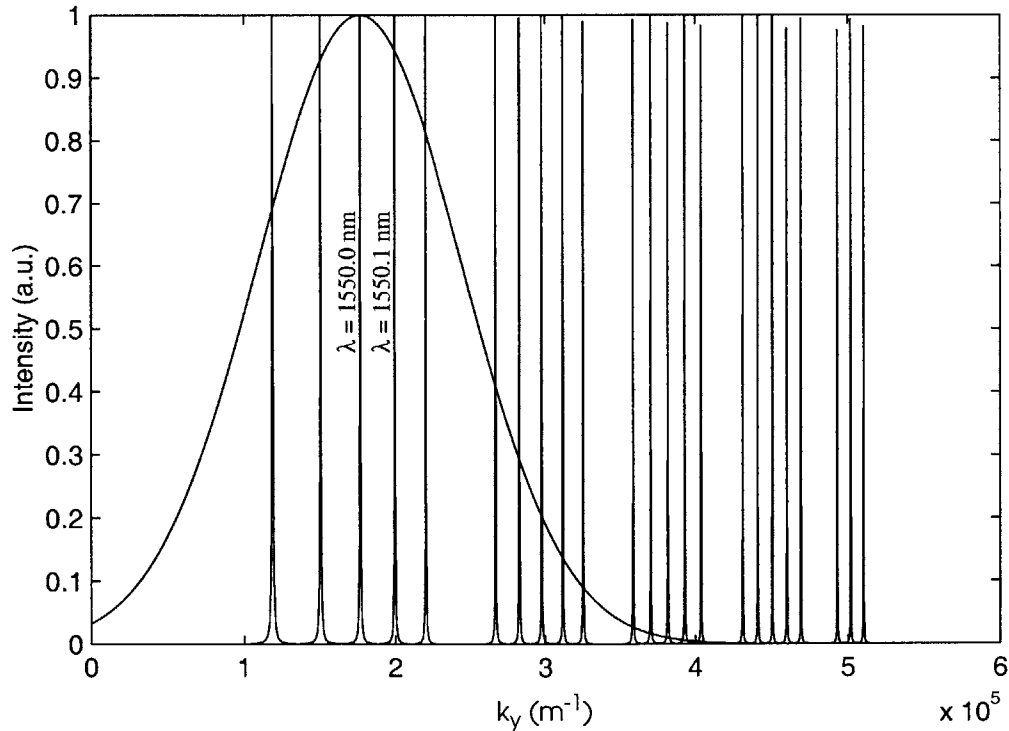
Figure 6-2: Far-field envelope and modulation

According to the ideal VIPA model, the highest intensity peak indeed occurs at the unde-flected wavelength. In general, as shown in FIGURE 4-2, the highest intensity peak occurs at a shorter wavelength. Unfortunately, power in the ideal formulation is not conserved, since the total power in each wavelength is not the same. For example, the lobes for $\lambda = 1550.1$ nm are always thinner and shorter than the lobes for $\lambda = 1550.0$ nm immediately to the left. Therefore, the integral of the power in the component lobes must be smaller. Since all wavelengths started with the same power, this would be a violation of energy conservation, so the ideal virtual image approximation is not valid. The invalidity arises from the effect of the window. Constructing the wavefront implied by the VIPA ideal is impossible. Fortunately, the simulation can predict the wavelength with the least lobe loss.

6.2 Transmission spectrum clipping at $\Theta = 2.8°$

For wide bandwidth configurations and $\Theta = 2.8°$, the bandwidth is actually more narrow than when $\Theta = 2.5°$. The transmission spectrum is clipped and falls off rapidly at shorter wavelengths (see FIGURE 6-3). This happens because of the appearance of non-negligible l_{-1} lobes.

$\Theta = 2.8°$ produces less dispersion than $\Theta = 2.5°$. Therefore, its lobes are closer together (see FIGURE 6-4). This causes more lobe loss at the band edge since the l_{-1} lobe appears sooner and grows rapidly. In narrow bandwidth cases, other loss mechanisms drown out this effect.
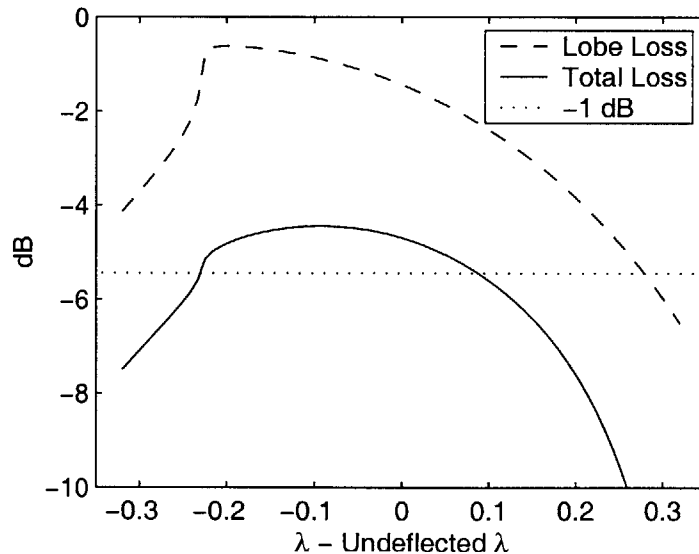
Figure 6-3: Transmission spectrum clipping at $\Theta = 2.8°$
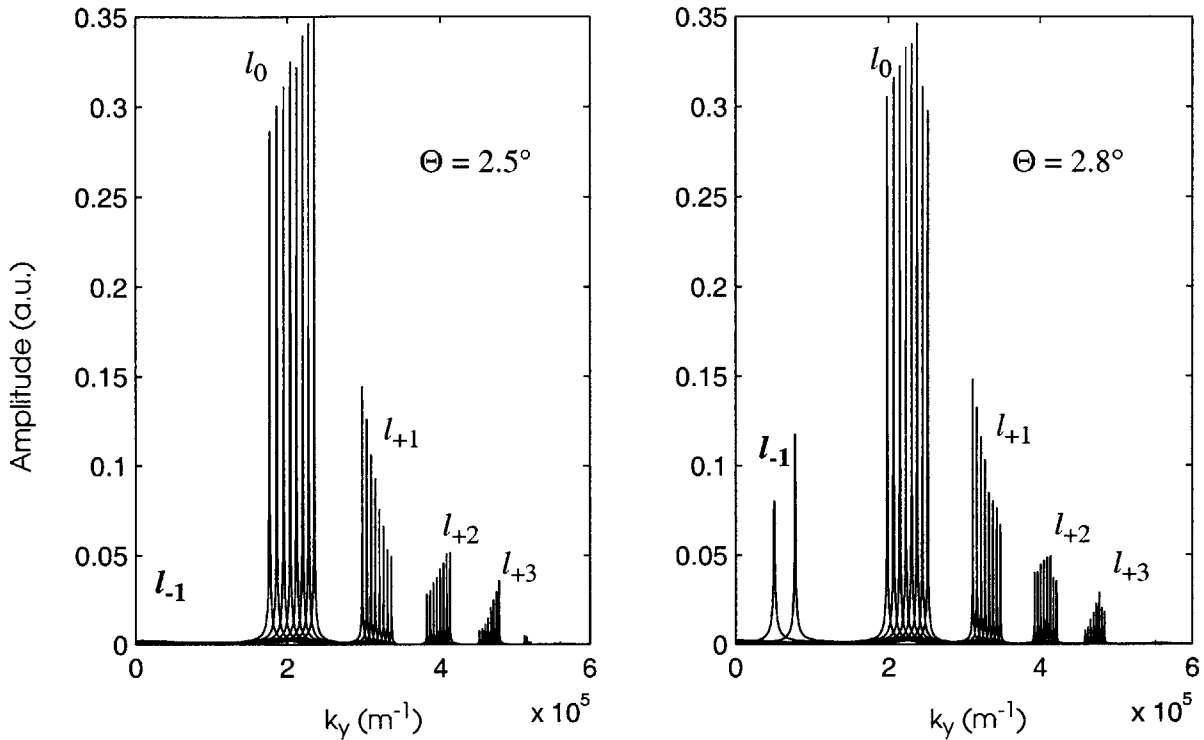
Figure 6-4: V_{Total} for $\lambda < 1550.0$ nm for $\Theta = 2.5°$ and $2.8°$

6.3 Secondary-lobe cross-talk

The profile of light at the mirror consists of multiple lobes. The VIPA compensator is intended to operate on only the main lobes (see SECTION 4.3). However, the other lobes cannot be ignored. They too can couple back into the optical fiber, and will cause cross-talk in the same channel since they represent different parts of the data stream from the main lobe. Since very little power will be concentrated in lobes of order greater than one, only the $l_{\pm 1}$ lobes need to be considered. The l_{+1} lobe is delayed with respect to the l_0 lobe and the l_{-1}
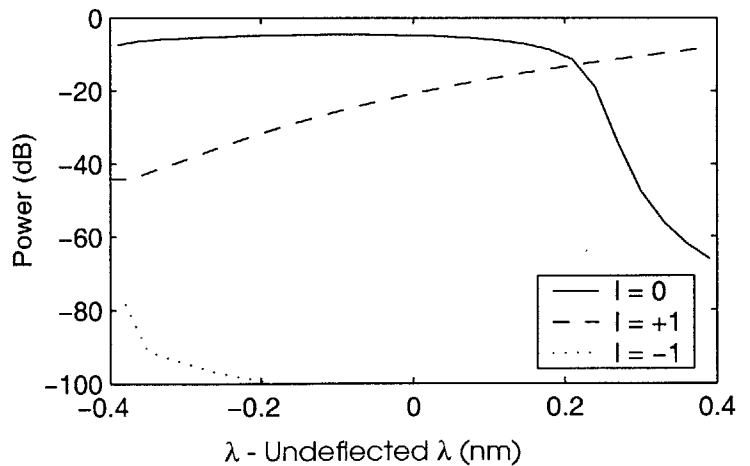
Figure 6-5: Secondary-lobe cross-talk

lobe is advanced with respect to the l_0 lobe. In either case, different parts of the data stream are superposed onto the main data stream. FIGURE 6-5 shows that the l_{+1} lobe power becomes comparable to the l_0 lobe power at the longer wavelength end of the channel. The l_{+1} lobe has very little power over the entire 0.8 nm channel, and can safely be ignored.

The mirror can eliminate this secondary lobe power by either deflecting it away or absorbing enough of it to reduce its coupling to negligible levels.

6.4 Mismatched constant dispersion mirror

The etalon tilting angle Θ and the thickness t of the etalon determine the center wavelength of the VIPA transmission spectrum. This wavelength must match the WDM channel center wavelength which is fixed by industry standard. There are two ways to tune the compensator to the correct center wavelength: adjusting t and adjusting Θ. The thickness can be changed by ele-
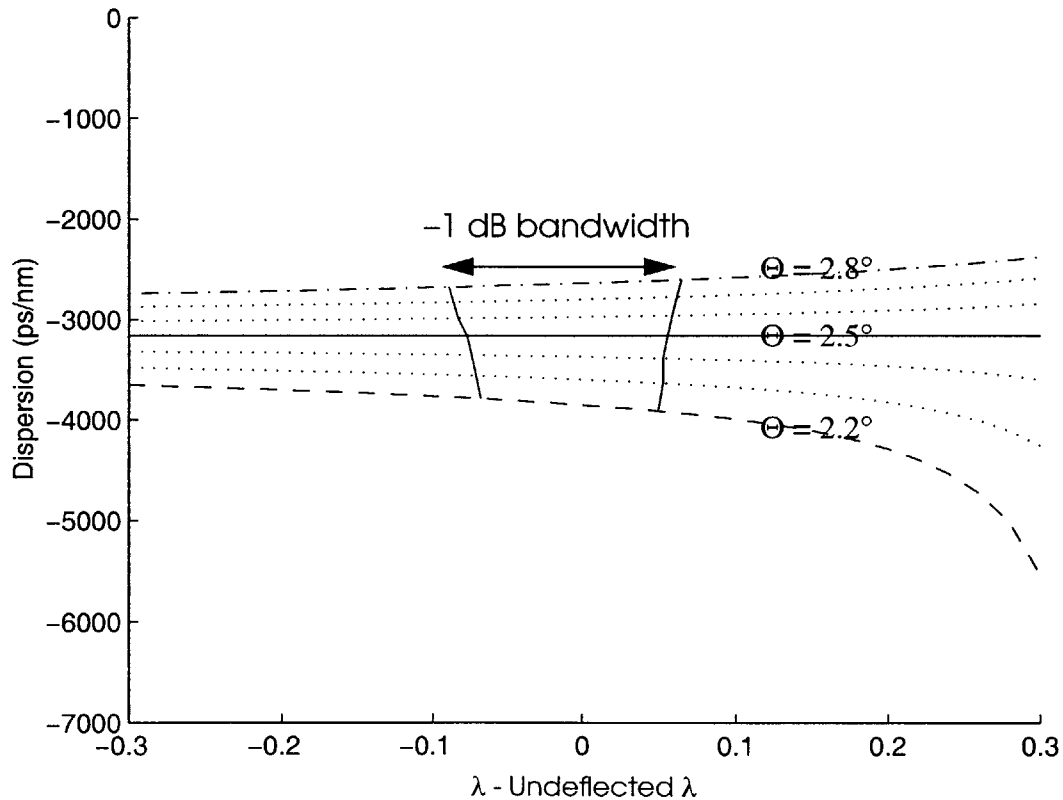
Figure 6-6: Mis-matched constant dispersion mirror

vating or reducing the temperature of the etalon. Alternatively, Θ can be adjusted to ensure that the center wavelength is in the middle of the compensator's transmission band. Varying Θ from 2.2° to 2.8° shifts the compensator's transmission band by approximately 2.1 nm. Without reprogrammability, a constant dispersion mirror designed for $\Theta = 2.5°$ may be mismatched when it is actually used (see FIGURE 6-6).

$$\frac{d\Phi}{d\lambda} \approx -\frac{n^2}{\lambda\Phi} \qquad [2.1]$$

$$\frac{d\lambda}{d\Phi} = \frac{\lambda\Phi}{n^2}$$

$$\frac{\Delta\lambda}{\Delta\Phi} = \frac{\lambda\Phi}{n^2}$$

$$\Delta\lambda = \frac{\lambda\Phi\Delta\Phi}{n^2}$$

Although the dispersion bias shifts, the normalized standard deviation of the dispersion σ_n remains very small (less than $\pm 2\%$) over the range of Θ. Also, the insertion loss stays low and the bandwidth does not decrease much below the matched case (see TABLE 6-1). The dispersion bias can be tuned, as discussed in SECTION 5-5, by varying l.

Table 6-1: Mismatched constant dispersion mirror[a]

Θ	Transmissivity	Mirror	Dispersion Bias	σ (ps/nm)	σ_n	Insertion Loss	Bandwidth
2.2°	40 %/cm	$K = 70$	-3,837 ps/nm	66	0.0171	-2.46 dB	0.12 nm
2.3°	40 %/cm	$K = 70$	-3,589 ps/nm	37	0.0104	-2.35 dB	0.12 nm
2.4°	40 %/cm	$K = 70$	-3,364 ps/nm	16	0.0047	-2.26 dB	0.13 nm
2.5°	40 %/cm	$K = 70$	-3,161 ps/nm	0.1235	3.907 E-5	-2.20 dB	0.13 nm
2.6°	40 %/cm	$K = 70$	-2,976 ps/nm	12	0.0040	-2.13 dB	0.14 nm
2.7°	40 %/cm	$K = 70$	-2,804 ps/nm	21	0.0076	-2.09 dB	0.15 nm
2.8°	40 %/cm	$K = 70$	-2,647 ps/nm	28	0.0107	-2.06 dB	0.15 nm

a. $\Theta = 2.5°$ is the matched case.

6.5 Thickness-mismatch in 2-level transmissivity coating

If the thickness of the transmissive coatings in the multi-level cases do not differ by an integer multiple of the propagating wavelength, then thickness-mismatch loss will occur. To simplify the analysis, assume only two coatings (phase difference δ corresponds to the thickness mismatch) and assume rectangular modes (height h and width w). Assume also that the mode width is independent of wavelength (see SECTION 6.6).
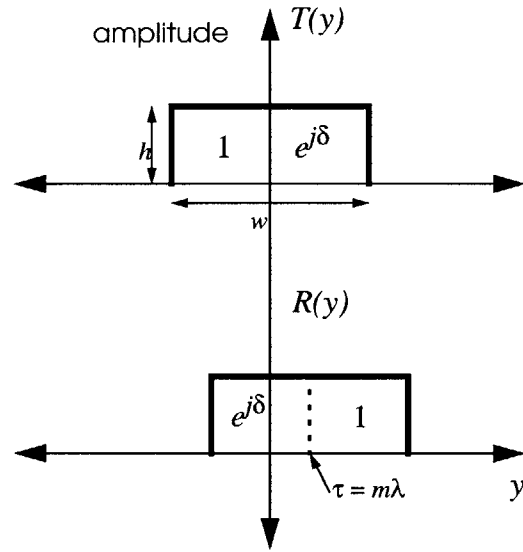
Figure 6-7: Simplified 2-level transmission and reflection modes with thickness-mismatch

If a constant dispersion mirror is used, then the lateral displacement τ of the reflection mode with respect to the lens axis will be linearly dependent on wavelength, with $\tau = m\lambda$ (see FIGURE 6-7). The coupling loss will be modified by the effect of the thickness-mismatch:

$$overlap = \int_{-\infty}^{\infty} TR dy$$

$$overlap = h^2 \left(\int_{-\frac{w}{2}+\tau}^{0} e^{j\delta} dy + \int_{0}^{\tau} 1 dy + \int_{\tau}^{\frac{w}{2}} e^{j\delta} dy \right)$$

$$overlap = h^2 ((w - 2|\tau|)e^{j\delta} + |\tau|)$$

$$couplingLoss = 1 - |overlap|^2 = 1 - h^4 ((w - 2|\tau|)^2 + 2|\tau|(w - 2|\tau|)\cos\delta + |\tau|^2)$$

For the 20%/cm template, K = 70, 2-level coating, the reflection mode translates ±5 mm over the wavelength range ∓ 0.3 nm ($m = -16.7$ mm/nm) and the transmission mode is 1.2 cm wide. A rectangular approximation might be $w = 1.0$ cm wide with h serving as a normalization constant.

62
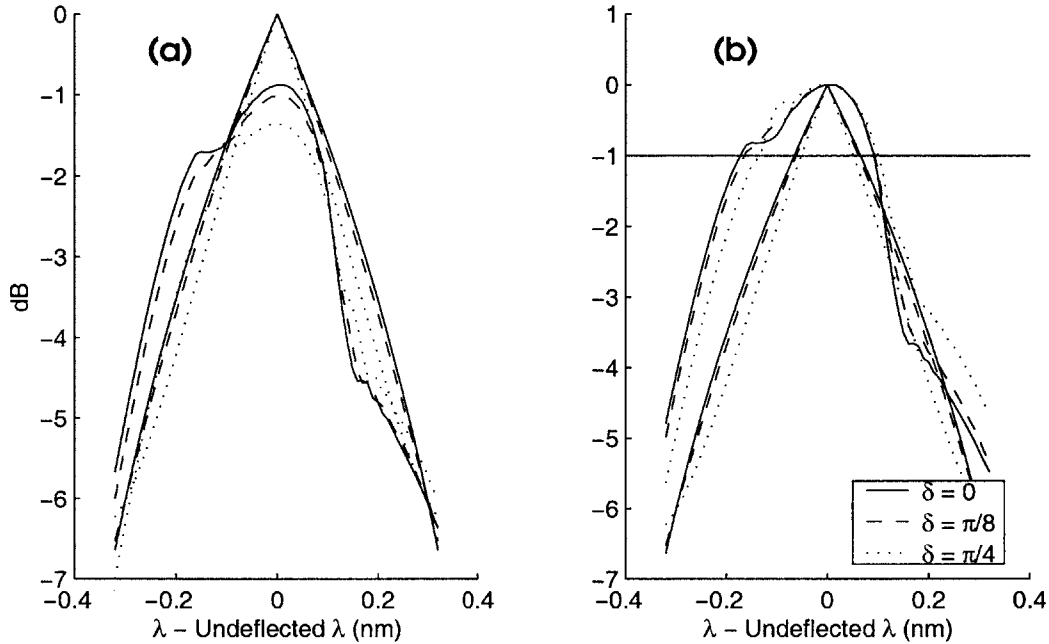
Figure 6-8: Simplified and numerical effects of thickness-mismatch
(a) Coupling loss spectra. **(b)** Coupling loss spectra shifted to isolate bandwidth change.

FIGURE 6-8 shows the simplified and simulated coupling loss for different thickness-mismatch between T_{Mode} and R_{Mode} for the 2-level configuration presented in SECTION 5.4. Since the more important effect is the change in bandwidth, FIGURE 6-8-b isolates the bandwidth difference from the coupling loss by shifting the simulated spectra upwards. The simplified representation is only useful as a gauge for the change in bandwidth as the thickness-mismatch between the two transmissive coatings is increased (see TABLE 6-2). The overall correspondence between the simulated and simplified coupling loss is poor but the simplified representation predicts the bandwidth degradation reasonably well. The system can easily tolerate a thickness-mismatch of as much as 100 nm, since $\delta = \pi/8$ translates to 100 nm in free space when $\lambda = 1550$ nm.

Table 6-2: Effects of 2-level coating phase mismatch

δ	Simulated bandwidth	change	Simplified bandwidth	change
0	0.262 nm	NA	0.131 nm	NA
$\pi/8$	0.253 nm	-0.009 nm	0.121 nm	-0.010 nm
$\pi/4$	0.229 nm	-0.033 nm	0.102 nm	-0.029 nm

6.6 Mode width wavelength dependence

One final observation that may not have any profound implications is that the modes of longer wavelengths are more narrow than the modes of shorter wavelengths. This phenomenon results from the system's geometry. Rays from longer wavelengths propagate closer to the etalon's normal, which means they are more closely spaced upon exit (see FIGURE 6-9). Therefore, their composite beams will be more narrow. This should mean that the coupling loss for longer wavelengths increases more quickly than for shorter ones when a constant dispersion mirror is used. Sharper roll-off at longer wavelengths was observed for the constant cases but not for the linear cases (see figures in SECTION 5). The modes for the constant cases are decreasing exponentials; this accounts for the asymmetry of the coupling loss spectrum. Since there is virtually no difference in roll-off between the longer and shorter wavelengths of the symmetric linear modes, the effect of mode narrowing over wavelength must be negligible for these modes.

blue modes are wider

red modes are narrower
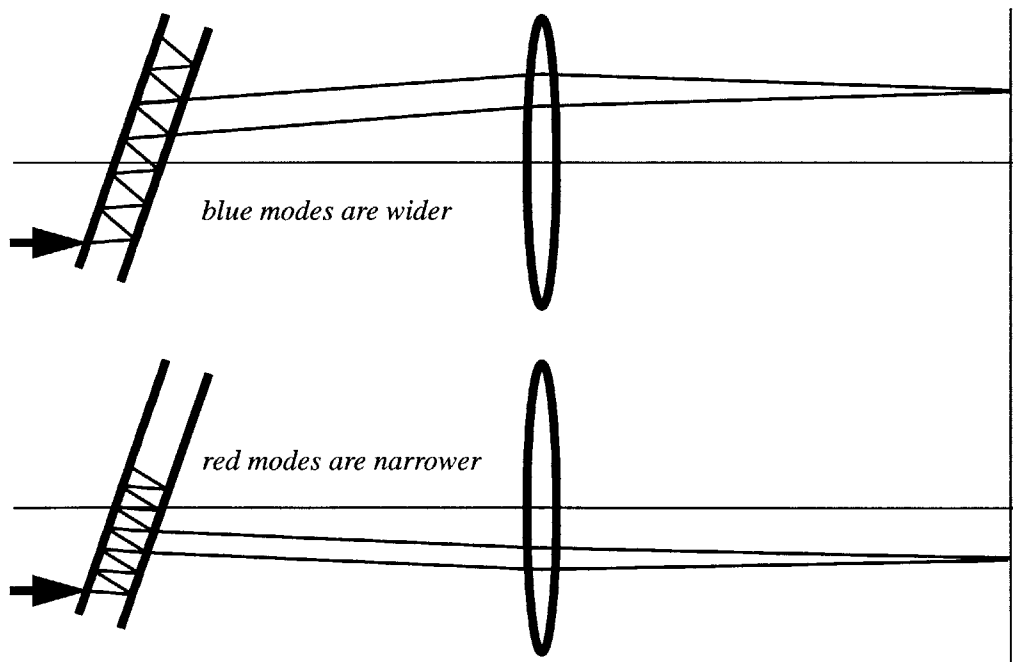
Figure 6-9: Ray spacing dependence on wavelength

7.0 Conclusions

Chromatic dispersion compensation using a virtually imaged phased array produces large dispersion with low loss. The FSR determines the index-thickness product, but higher index etalons are better. The tilt of the etalon, in conjunction with the mirror shape, controls the dispersion bias. Larger dispersion bias translates to lower bandwidth, but does not affect the insertion loss. The shape of the mirror controls the dispersion profile and arbitrary dispersion profiles including constant dispersion can be produced. The transmissive coating determines the insertion loss as well as the bandwidth. Constant coatings provide wide bandwidth but suffer from high insertion loss. Linear coatings exhibit low insertion loss but have narrow bandwidth. The 2-level coating is superior to both since it features low insertion loss and wide bandwidth. The 3-level coating places a trough in the center of its transmission spectrum which would increase the effective bandwidth of the VIPA compensator cascaded with other modules. Finally, the VIPA compensator is tunable over a large range with very little mechanical displacement.

Ray optics is enough to predict the dispersion bias and shape of the VIPA compensator. However, the insertion loss and bandwidth can only be predicted by numerical simulation. The simulations also proved useful in analyzing a number of non-idealities. Since the VIPA approximation is not valid for predicting the far-field pattern, the undeflected wavelength is not in the center of the transmission band. Wide bandwidth configurations with low dispersion are subject to spectral clipping at large etalon tilt angles. Cross-talk between higher order lobes and the main lobe is non-negligible at long wavelengths. Changing the etalon tilt can compensate for manufacturing variations in the thickness of the etalon without substantially degrading the compensator's performance. Finally, the VIPA compensator can tolerate moderate thickness-mismatch between the coatings in the 2-level case.

References

[1] M. Shirasaki.
"Chromatic-Dispersion Compensator Using Virtually Imaged Phased Array"
IEEE Photonics Technology Letters, vol. 9, no. 12, pp 1598, 1997.

[2] M. Shirasaki, H. Isono, S. Cao.
"Dispersion compensation using the virtually imaged phased array"
Proceedings, OECC 1999, pp 1367-1370.

[3] C. Lin, H. Kogelnik, L. G. Cohen.
"Optical-pulse equalization of low-dispersion transmission in single-mode fibers in the 1.3-
1.7 mm spectral region"
Optics Letters, vol. 5, no.11, pp 476-478, 1980.

[4] F. Ouellette.
"Dispersion cancellation using linearly chirped Bragg grating filters in optical waveguides"
Optics Letters, vol. 12, no. 10, pp 847-849, 1987.

[5] M. Shirasaki.
"Large angular dispersion by a virtually imaged phased array and its application to a wave-
length demultiplexer"
Optics Letters, vol. 21, no. 5, pp 366, 1996.

[6] A. N. Akhter, C. Lin, M. Shirasaki.
"A Method for Correcting Effects of a Non-uniform Plate in a VIPA system"
1999 OSA Annual Meeting and Exhibit, p. 121.

[7] M. Shirasaki, A. N. Akhter, C. Lin.
"Virtually imaged Phased Array with Graded Reflectivity"
IEEE Photonics Technology Letters, vol. 11, no. 11, pp 1443, 1999.

[8] H. A. Haus.
Waves and Fields in Optoelectronics
Prentice-Hall, Inc., Englewood Cliffs. © 1984.

[9] L. D. Garret, A. H. Gnauck, M. H. Eiselt, R. W. Tkach, C. Yang, C. Mao, S. Cao.
"Demonstration of virtually-imaged phased-array device for tunable dispersion compensation
in 16 x 10 Gb/s WDM transmission over 480 km standard fiber"
Technical Digest, OFC 2000, PD7.

Appendix A: Experimental Corroboration

The VIPA compensator is currently being commercially developed. The simple constant coating design is the only one that has ever been built. The first published experimental results for this design appear in [1] by M. Shirasaki published in 1997. In that paper, Shirasaki shows an eye diagram demonstrating improvement of a dispersed signal (1800 ps/nm) after passing through the VIPA compensator. Shirasaki also measured 0.4 nm for the −1 dB bandwidth, −13 dB insertion loss, and very low polarization dependence (only 0.1 dB). As expected, Shirasaki observed no nonlinear effects. The high insertion loss was primarily due to misalignments.

More recently, Shirasaki (*et al.*) published more refined results in [2]. Included is a measurement of group delay that is reproduced here with permission (see FIGURE A-1). Oddly enough, the apparent error between the numerical and theoretical estimates of group delay is reproduced in the experiment. Perhaps the simulation is capturing some real effect that is not represented in the theory. The experimental measurement, which repeated every 0.8 nm, corresponds well with the simulated results.
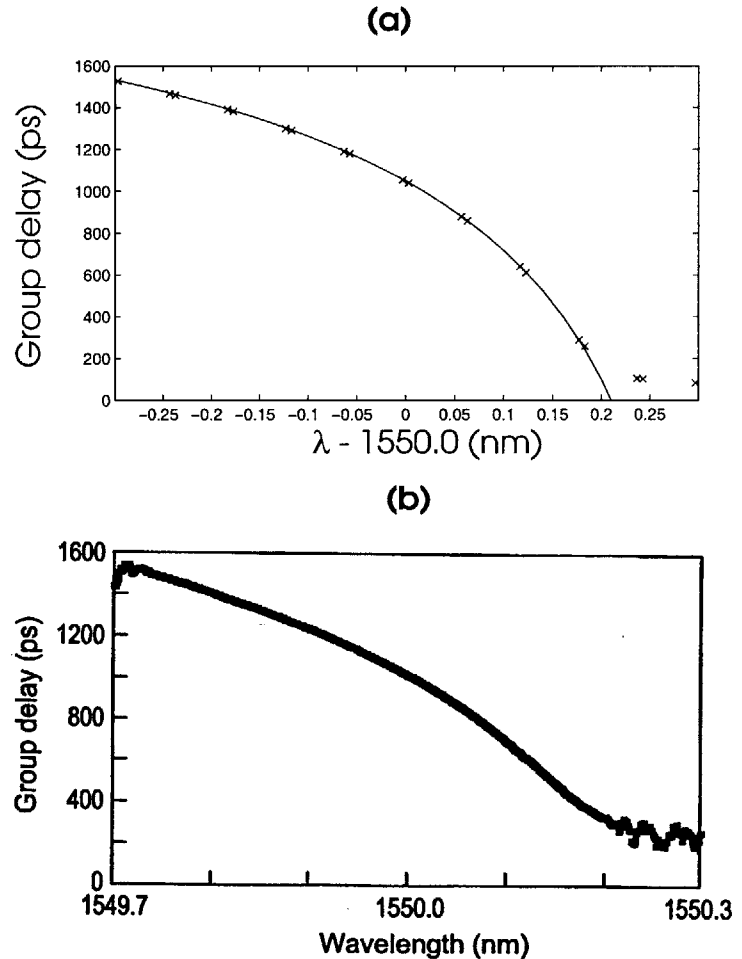
Figure A-1: Experimental and simulated group delay
(a) Numerical (symbols) and theoretical (line).
(b) Experimental results reproduced with permission (2).

The authors also demonstrated tunability over a 4000 ps/nm range by varying the distance between the lens and the etalon. Finally, they measured −7 dB insertion loss, which is close to the simulated loss (−4.5 dB) if the isolator and collimator losses (−1.5 dB) are included and the reflective mirror is assumed to be 99.9% reflective instead of perfectly reflective (−1.0 dB) for a simulated total of approximately −7 dB.

The most recent and most extensive demonstration to date was performed by Garret (*et al.*) from AT&T Laboratories in conjunction with Yang (*et al.*) at Avanex Corporation [9]. These researchers ran the VIPA compensator against DCF in an 80 km loop complete with an erbium doped fiber amplifier six times, for a total transmission distance of 480 km. The VIPA compensator module was compact: measuring only 1 in. by 1 in. by 4.5 in. They were able to tune it from −1100 ps/nm to −1500 ps/nm and simultaneously operate on 16 WDM channels spaced 0.8 nm apart. They measured an insertion loss of −9 dB for the VIPA compensator and −12 dB for the DCF. These were the best-case channels for each approach, and the VIPA exceeded the performance of the DCF by an average of 0.85 dB over all 16 channels.

These loss figures do not represent the full potential of the VIPA compensator. The loss figure for DCF increases as the amount of corrective dispersion increases. For the VIPA compensator, on the other hand, insertion loss stays fixed regardless of dispersion. Bandwidth is reduced, but insertion loss is unaffected. As shown in this thesis, the VIPA can easily produce twice as much dispersion as Garret (*et al.*) configured it to produce. This means the VIPA compensator should only appear in every other loop so that overall, it introduces approximately half as much loss as the DCF.

Appendix B: Application to Polarization Mode Dispersion

In polarization mode dispersion (PMD), the objective is to introduce different group delays on the order of 20 ps or so without chromatic dispersion in the two different polarization modes. The VIPA compensator can be configured to do this by designing it so that $a = f$. With a flat mirror, this corresponds to zero chromatic dispersion since $h(y) = 0$ and $(f-a) = 0$:

$$D = -\frac{2n^4}{c\lambda\Phi^3}\left[(f-a)\Phi + f^2\Phi\frac{d}{dy}h(y) - fh(y)\right] \qquad [2.5]$$

$$D = -\frac{2n^4}{c\lambda\Phi^3}\{(f-a)\Phi\}$$

A PMD compensator would have two VIPA compensators in parallel: one for each polarization. To introduce the differential group delay, the distance between the focusing lens and etalon (the value of a) in one of the VIPA compensators would be changed. Doing so produces chromatic dispersion, but the amount of chromatic dispersion is small. However, EQUATION 2.4 is insufficient for predicting the differential group delay as a function of a since it reduces to zero when $\Phi = \Theta$:

$$G = \frac{2n^2}{c\Phi}[(f-a)(\Phi-\Theta) + fh(y)] \qquad [2.4]$$

$$G = \frac{2n^2}{c\Phi}\{(f-a)(\Phi-\Theta)\} = 0$$

In order to analyze the PMD application, the term ignored when deriving EQUATION 2.4 from EQUATION 2.3 must be reconsidered:

$$\gamma \approx \frac{2\pi}{\lambda}\{2(f+a)+(f-a)(\Phi-\Theta)^2+2c(y)\} \qquad [2.3]$$

$$G = \frac{d\gamma}{d\omega} = \frac{-\lambda^2}{2\pi c}\frac{d\gamma}{d\lambda}$$

$$G = \frac{2(f+a)+(f-a)(\Phi-\Theta)^2+2c(y)}{c} - \frac{2\lambda}{c}\left[(f-a)(\Phi-\Theta)+h(y)\frac{dy}{d\Phi}\right]\frac{d\Phi}{d\lambda}$$

$$G = \frac{2(f+a)+(f-a)(\Phi-\Theta)^2}{c}$$

$$G = \frac{2(f+a)}{c}$$

For $f = 5$ cm and a biased at 5 cm, 20 ps of differential group delay can be achieved by varying a by only 3 mm.

Alternatively, the group delay in one of the arms could be changed by tilting the flat mirror. For a flat mirror, $h(y)$ is constant and a tilt corresponds to changing the constant value of $h(y)$. Using this method yields:

$$G = \frac{2n^2}{c\Phi}fh(y)$$

$$\tan\xi = h(y)$$

Assuming $\Phi = 2.5°$, tilting the mirror by the angle $\xi = 0.05°$ would introduce 20 ps of differential group delay to one of the polarizations.

Appendix C: Simulation Code

These are the files that comprise the VIPA chromatic dispersion compensator simulator.

The file "`chromatic.m`" is the main script and runs the other sub-programs in sequence. Lines

of code preceded by "%" are commented (not run) and lines indented into the middle of the page

and preceded by "\" are continuations of the previous line.

chromatic.m
```
% Chromatic Dispersion Compensation Master Template Function
% by Christopher Lin
% Last modified 2/29/1999
% This is the main script that runs all of the other ones.

ttl = 'Angle, Transmissivity, Mirror, Other'

params

lambda

total

cmT

mirror

cmVmR

cdisp

cspecs

plots
```

params.m
```
% This file sets all of the system variables except for the
% wavelengths (see lambda.m) and the details of the mirror
% (see mirror.m).


n= 1.8;                                  % refractive index of glass
f = 0.05                                 % 5cm focal length
l = 0.005                                % 5mm btwn plate and lens
thetaAir    = 2.5*pi/180
thetaGlass = asin(sin(thetaAir)/n)
m = 1858
t = 800.2072e-6                          % plate thickness
% t = m*1.55e-6/(2*n*cos(thetaGlass));   % plate thickness formula

points = 1024 * 4                        % num points on axes
scale = 4                                % zero-padding parameter

% y axis, length = 100000 microns
% The y axis is zero padded to 10cm in order to improve fft resolution
```

```
ky = zeros([1,points]);
yT = linspace(0,100000e-6,points*scale);    y  = yT(1:points);
deltay = y(2) - y(1)
yo = 500e-6                                  % location of window edge

RL = ones([1,points]);                       % reflection coeff on left
RR = ones([1,points]);                       % reflection coeff on right

% create reflective side mirror

for ir=1:points,
    if(y(ir)< yo)
        RL(ir)=0;
    else RL(ir)=1;
    end
end

% create transmissive side mirror
% three possibilities: constant, linear, and step

%%%%% uniform reflectivity on right side
% RR = sqrt(.98) * RR;
% T  = sqrt(1- .98);

%%%%% linear transmissivity depends on points
%TRamp = zeros([1,points]);
%TRlow = 0;
%TRhi  = 1;
%delTR = (TRhi- TRlow)/(points);
%tmp   = 0;

%for it = 1:points,
%    if (y(it) <= yo)
%        TRamp(it) = 0;
%        tmp = it;
%    else
%        TRamp(it) = delTR * (it - tmp);
%    end
%end

%for it = 1:points,
%    if (TRamp(it)>1)
%        TRamp(it)=1;
%    end
%end

%RR = sqrt(1 - TRamp.^2);
%T  = TRamp;

%%%%% step transmissivity
T = zeros([1,points]);

for it = 1:points,
    if (y(it) <= (yo+0.003333))
        T(it) = sqrt(0.0089);
    elseif (y(it) <= (yo+0.006667))
        T(it) = sqrt(0.0444);
    else
        T(it) = sqrt(0.1156);
    end
end

RR = sqrt(1 - T.^2);
```

lambda.m

```
%Builds master wavelength related vectors.

noWvl = 13 % must be odd
res   = 5    % must be odd
midLambda   = (noWvl+1)/2;
exmidLambda = (noWvl*res+1)/2;

% fundamental wavelengths

minLambda = 1.5497e-6
maxLambda = 1.5503e-6
lambdaAir = zeros(1,noWvl);
lambdaAir = linspace(minLambda,maxLambda,noWvl);

% Set spacing between fundamental wavelengths and auxiliary
% wavelengths that are carried along in order to compute
% derivatives. Larger dlAir decreases numerical noise but
% increases the likelihood of 2*pi phase differences that
% are difficult to correct using software.

dlAir = 0.005e-9

exlAir   = zeros(1,noWvl*res);
exlGlass = zeros(1,noWvl*res);

% generate auxilliary wavelengths according to fundamental
% wavelengths and dlAir

for(ii=1:noWvl)
    exlAir((ii-1)*res+1:(ii-1)*res+res) = linspace((lambdaAir(ii)-dlAir*(res-1)/2),
                                    \(lambdaAir(ii) +dlAir*(res-1)/2),res);
end

exlGlass = exlAir/n;

lambdaGlass = zeros(1,noWvl);
lambdaGlass = lambdaAir/n;

kair = zeros(1,noWvl);
exkair = zeros(1,noWvl*res);
kair   = 2*pi./lambdaAir;
exkair = 2*pi./exlAir;

kglass   = zeros(1,noWvl);
exkglass = zeros(1,noWvl*res);
kglass   = kair*n;
exkglass = exkair*n;
```

total.m

```
wo = sqrt(lambdaGlass(midLambda)*t/pi)          % (meters)

noRefl = 400                                     % number of reflections calculated
UL = zeros([1,points]);                          % gaussn magnitude profiles on left
UR = zeros([1,points]);                          % gaussn magnitude profiles on right

VL = zeros([1,points]);                          % fft coeffs on left
VR = zeros([1,points]);                          % fft coeffs on right

UR_ideal = zeros([1,points]);
VR_ideal = zeros([1,points]);

Utotal  = zeros([noWvl*res,points]);
ULtotal = zeros([noWvl*res,points]);
```

```
Ttotal  = zeros([noWvl*res,points]);
Vtotal  = zeros([noWvl*res,points *scale]);          % with zero padding

kyg = zeros([1,noWvl]);
ky  = (linspace(0,2*pi,points))/ deltay;
kyT = (linspace(0, 2*pi ,(points *scale)))/ deltay;

% plateEff corresponds to etalon efficiency

windowEff    = zeros(noWvl*res,1);
plateEff     = zeros(noWvl*res,1);
lobeEff      = zeros(noWvl*res,1);
lobeRatio    = zeros(noWvl*res,1);
couplingEff  = zeros(noWvl*res,1);
efficiency   = zeros(noWvl*res,5);

for j=1:noWvl*res
    kyg(j) = exkglass(j) * sin(thetaGlass)  ;
    Uphase = exp(i* (y -yo) * kyg(j));               % linear phase due to incl

% --------------------PHASE FACTOR FOR PROG TO RIGHT--------------------
% all phase factors must be reconstructed as shown to be compatible with
% discrete computation

    p_fac= exp((i*(exkglass(j)*t)).*(1-(0.5*((ky/exkglass(j)).^2))));
    phase_fac = [p_fac(1:points/2) fliplr(p_fac(2:(points/2+1)))];

% --------------------PHASE FACTOR FOR PROG TO LEFT--------------------

    p_fac_init= exp((i*(exkglass(j)*(-t))).*(1 -(0.5*((ky/exkglass(j)).^2))));
    phase_fac_init = [p_fac_init(1:points/2) fliplr(p_fac_init(2:(points/2+1)))];

% ------------------------------------------------

% ideal gaussians at z=0 %

    UR_ideal = exp(-1 *((y - yo).^2)/(wo^2)) .* Uphase ;

%%%% initial profiles at z= -t %

    U_init = ifft(fft(UR_ideal) .* phase_fac_init);
    A = sqrt(1/sum(abs(U_init).^2));
    U_init_left = A*(1- RL) .* U_init;

    windowEff(j) = sum(abs(U_init_left).^2);

%%%% adjusted profiles at z = 0 %

    UR = ifft(fft(U_init_left) .* phase_fac);
    B  = sqrt(1/sum(abs(UR).^2));
    UR = B*UR;
    UL = ifft((fft(RR .* UR)) .* phase_fac);
    Utotal(j,:)  = Utotal(j,:)  + UR;
    ULtotal(j,:) = ULtotal(j,:) + UL;

%%% total profile for each wavlength w/o zero padding%%

    for kk= 2:noRefl,
        UR = ifft(fft(RL .* UL).* phase_fac);
        UL = ifft(fft(RR .* UR).* phase_fac);
        Utotal(j,:)  = Utotal(j,:)  + UR;
        ULtotal(j,:) = ULtotal(j,:) + UL;
    end

    Ttotal(j,:) = T.*Utotal(j,:);
```

```
    plateEff(j) = sum(abs(Ttotal(j,:)).^2);

% zero-pad fft to improve frequency domain resolution

    Vtotal(j,:) = fft(Ttotal(j,:), points *scale);

    C = sqrt(1/sum(abs(Vtotal(j,:)).^2));
    Vtotal(j,:) = C*Vtotal(j,:);
end

UL = zeros(1,1);
UR = zeros(1,1);

% Power efficiencies must be squared to account
% for return path loss through the same mechanism.

windowEff = windowEff.^2;
plateEff  = plateEff.^2;
```

cmT.m

```
%%%%% locate mode maxima

Mvt = zeros(noWvl*res,1);
Ivt = zeros(noWvl*res,1);

Mv = zeros(noWvl*res,1);
Iv = zeros(noWvl*res,1);

[Mvt(exmidLambda),Ivt(exmidLambda)] = max((abs(Vtotal(exmidLambda,:))));

% This loop ensures that the main lobes of other wavelengths
% are positioned correctly relative to the main lobe of the
% undeflected wavelength (midLambda). Longer wavelengths must
% be to the left of midLambda and shorter wavelengths must be
% to the right.

for ii=1:noWvl*res
    if(ii>exmidLambda)
        [Mvt(ii),Ivt(ii)] = max((abs(Vtotal(ii,1:Ivt(ii-1)))));
    elseif(ii<exmidLambda)
        [Mvt(exmidLambda-ii),Ivt(exmidLambda-ii)] = max((abs(Vtotal((exmidLambda-ii),
                                    \Ivt(exmidLambda+1-ii):(points*scale)))));
        Ivt(exmidLambda-ii) = Ivt(exmidLambda-ii) + Ivt(exmidLambda+1-ii);
    end
end

Vmain = zeros(noWvl*res,points*scale);
Tmain = zeros(noWvl*res,points*scale);
% Computation of phaseTmain needed only for diagnostic purposes.
% That's no longer necessary, so all related code has been
% commented out since phase computations are very slow.
%phaseTmain = zeros(noWvl*res,points*scale);

% Need to extract Vmain from Vtotal. Lobes for different wavelengths
% have different thicknesses and spacings. Shorter wavelength lobes
% are generally thinner and spaced closer together. rangeS is smaller
% than range to ensure that other lobes are not accidentally included
% in Vmain. range is large enough to ensure that long wavelength main
% lobes are extracted in their entirety.

range = points*scale/16;
rangeS = points*scale/32;
```

```
for ii=1:noWvl*res
    if(exlAir(ii)<1549.75e-9)
        if( (Ivt(ii)-rangeS)<1)
            Vmain(ii,1:(Ivt(ii)+rangeS)) = Vtotal(ii,1:(Ivt(ii)+rangeS));
            Vmain(ii,(points*scale+Ivt(ii)-rangeS):points*scale) =
                                \Vtotal(ii,(points*scale+Ivt(ii)-rangeS):points*scale);
        else
            Vmain(ii,(Ivt(ii)-rangeS):(Ivt(ii)+rangeS)) =
                                \Vtotal(ii,(Ivt(ii)-rangeS):(Ivt(ii)+rangeS));
        end
    else
        if( (Ivt(ii)-range)<1)
            Vmain(ii,1:(Ivt(ii)+range)) = Vtotal(ii,1:(Ivt(ii)+range));
            Vmain(ii,(points*scale+Ivt(ii)-range):points*scale) =
                                \Vtotal(ii,(points*scale+Ivt(ii)-range):points*scale);
        else
            Vmain(ii,(Ivt(ii)-range):(Ivt(ii)+range)) =
                                \Vtotal(ii,(Ivt(ii)-range):(Ivt(ii)+range));
        end
    end

    lobeEff(ii) = sum(abs(Vmain(ii,:)).^2);

    Tmain(ii,:) = ifft(Vmain(ii,:));

    D = sqrt(1/sum(abs(Tmain(ii,:)).^2));
    Tmain(ii,:) = D*Tmain(ii,:);



%    phaseTmain(ii,:) = phase(Tmain(ii,:));
end

% determine power center of undeflected wavelength transmission mode

dummy = 0;
[dummy,index] = max(abs(conv(Tmain(exmidLambda,:),Tmain(exmidLambda,:))))
center = round(index/2)

a = (center*deltay-yo)/(sin(thetaGlass)*n)+1

% compute phi from phaseTmain (troubleshooting)
%phi = zeros(noWvl*res,1);
%phiRelative = zeros(noWvl*res,1);

%rangeP=points*scale/512;
%for ii = 1:noWvl*res
%    phi(ii) = asin((phaseTmain(ii,(center-rangeP))-phaseTmain(ii,(center+rangeP)))/
                                \(yT(center-rangeP)-yT(center+rangeP))/exkair(ii));
%end

% rotate Tmain to account for tilt of etalon
% (want midLamdba Tmain normally incident on lens)
% and center so that power center location is
% the first element of the Tmain vectors. This
% makes thinking about the fft more intuitive.

for ii=1:noWvl*res
%    phiRelative(ii) = phi(ii) - thetaAir;
    Tmain(ii,:) = Tmain(ii,:).*exp(-i*yT*sin(thetaAir)*exkair(ii));
    Tmain(ii,:) = [Tmain(ii,(center+1):points*scale) Tmain(ii,1:center)];
end

Mt = zeros(noWvl*res,1);
It = zeros(noWvl*res,1);
```

```
Mr = zeros(noWvl*res,1);
Ir = zeros(noWvl*res,1);

% to locate transmission lobe maximum

for ii=1:noWvl*res
    [Mt(ii),It(ii)] = max(abs(Tmain(ii,:)));
    [Mv(ii),Iv(ii)] = max(abs(Vmain(ii,:)));
end

% lobe loss happens twice and must be squared

lobeEff = lobeEff.^2;
lobeRatio = lobeEff/lobeEff(exmidLambda)
```

mirror.m

```
% There are two different kinds of mirrors:
% parabolic and constant dispersion. If the
% mirror is changed here, cdisp.m must also
% be updated.

tY   = zeros(1,points*scale);
ckyT = zeros(noWvl*res,points*scale);
hkyT = zeros(noWvl*res,points*scale);
mirr = ones(noWvl*res,points*scale);

r = 0.03

for ii=1:noWvl*res
    tY        = [kyT(1:points*scale/2) -fliplr(kyT(2:(points*scale/2+1)))]*f/exkair(ii);
    ckyT(ii,:) = tY.^2/(2*r);
    hkyT(ii,:) = tY/r;
    mirr(ii,:) = exp(i*2*exkair(ii)*ckyT(ii,:));
end

%K = 70;

%for ii = 1:noWvl*res
%    tY        = [kyT(1:points*scale/2) -fliplr(kyT(2:(points*scale/2+1)))]*f/exkair(ii);
%    ckyT(ii,:) = K/(8*f^4)*tY.^4 +  K*thetaAir/(2*f^3)*tY.^3 + (K*thetaAir^2-(f-a))/(2*f^2)*tY.^2;
%    hkyT(ii,:) = K/(2*f^4)*tY.^3 +3*K*thetaAir/(2*f^3)*tY.^2 + (K*thetaAir^2-(f-a))/(1*f^2)*tY;
%    mirr(ii,:) = exp(i*2*exkair(ii)*ckyT(ii,:));
%end
```

cmVmR.m

```
Vmain = zeros(noWvl*res,points*scale);
Rmain = zeros(noWvl*res,points*scale);

phaseBuffer = zeros(1,points*scale);

for ii=1:noWvl*res
% phase advance of Tmain from etalon to lens and back
    phaseBuffer = exp(i*(1*cos(kyT/exkair(ii))+f./cos(kyT/exkair(ii)))*exkair(ii));
    phaseBuffer = [phaseBuffer(1:points*scale/2) fliplr(phaseBuffer(2:points*scale/2+1))];
    Vmain(ii,:) = fft(Tmain(ii,:)).*phaseBuffer.*mirr(ii,:);

% re-center all R and T modes w.r.t. middle of y-axis
    Rmain(ii,:) = fft(Vmain(ii,:).*phaseBuffer);
    E = sqrt(1/sum(abs(Rmain(ii,:)).^2));
    Rmain(ii,:) = E*Rmain(ii,:);
    Tmain(ii,:) = [Tmain(ii,(points*scale/2+1):(points*scale)) Tmain(ii,1:(points*scale/2))];
    Rmain(ii,:) = [Rmain(ii,(points*scale/2+1):(points*scale)) Rmain(ii,1:(points*scale/2))];
    Vmain(ii,:) = [Vmain(ii,(points*scale/2+1):(points*scale)) Vmain(ii,1:(points*scale/2))];
```

```matlab
    [Mv(ii),Iv(ii)] = max((abs(Vmain(ii,:))));
end


gamma = zeros(noWvl*res,1);


% rotate Tmain and Rmain so they lie along the surface of etalon


for ii =1:noWvl*res
    Tmain(ii,:) = Tmain(ii,:).*exp(i*yT*sin(thetaAir)*exkair(ii));
    Rmain(ii,:) = Rmain(ii,:).*exp(-i*yT*sin(thetaAir)*exkair(ii));
% unfortunate oversight: here couplingEff corresponds to "overlap"
% overlap only calculated where non-zero data is expected
    couplingEff(ii) =  sum(Tmain(ii,(7*points*scale/16):(11*points*scale/16)).*
                                    \Rmain(ii,(7*points*scale/16):(11*points*scale/16)));
end


for ii=1:noWvl*res
    [Mv(ii),Iv(ii)] = max((abs(Vmain(ii,:))));
    [Mr(ii),Ir(ii)] = max((abs(Rmain(ii,:))));
    [Mt(ii),It(ii)] = max((abs(Tmain(ii,:))));
end


% interpreter is picky about input data to phase function


% variable couplingEff recycled
gamma = transpose(phase(transpose(couplingEff)))
couplingEff =  abs(couplingEff).^2;


totalEff = windowEff.*plateEff.*lobeEff.*couplingEff;
efficiency = [windowEff plateEff lobeEff couplingEff totalEff]
```

cdisp.m
```matlab
% must be updated if mirror.m is changed
% computes numerical and theoretical
% group delay and dispersion


% theoretical wavelengths spaced at 0.01 over numerical range
% statistics interpreted w.r.t. this spacing
noThe = round((maxLambda-minLambda)*100000000000+1);
lambdaThe = linspace(minLambda,maxLambda,noThe);
lambdaGD = zeros(noWvl*2,1);
phiThe = zeros(noThe,1);
gdThe = zeros(noThe,1);
dispersionThe = zeros(noThe,1);
h = zeros(noThe,1);
dhdy = zeros(noThe,1);


dispersionNum = zeros(noWvl-2,1);


groupDelay = zeros(noWvl*2,1);


c = 3e8; % speed of light in meters/picoseconds


%%%%% Parabolic Mirror
for ii = 1:noThe
    phiThe(ii) = acos((m*lambdaThe(ii)/n)/(2*t))*n;
    Y = f*(phiThe(ii)-thetaAir);
    h(ii) =      Y/r;
    dhdy(ii) = 1/r;
    gdThe(ii) = 2*n^2/(c*phiThe(ii))*((f-a)*(phiThe(ii)-thetaAir)+f*h(ii));
    dispersionThe(ii) = -2*n^4/(c*lambdaThe(ii)*phiThe(ii)^3)*((f-a)*thetaAir+f^2*phiThe(ii)*
                                    \dhdy(ii)-f*h(ii))*1000;
end
```

```matlab
for ii = 1:noWvl
    groupDelay(2*ii-1) = -(lambdaAir(ii)^2)/(2*pi*c)*(gamma(ii*res-(res-1)/2)-
                                       \gamma(ii*res-res+1))/(dlAir*(res-1)/2);
    groupDelay(2*ii)   = -(lambdaAir(ii)^2)/(2*pi*c)*(gamma(ii*res)-
                                       \gamma(ii*res-(res-1)/2))/(dlAir*(res-1)/2);
    lambdaGD(2*ii-1) = lambdaAir(ii) - (res-1)/4*dlAir;
    lambdaGD(2*ii)   = lambdaAir(ii) + (res-1)/4*dlAir;
end

%%%%% Constant Dispersion Mirror
%for ii = 1:noThe
%    phiThe(ii) = acos((m*lambdaThe(ii)/n)/(2*t))*n;
%    Y = f*(phiThe(ii)-thetaAir);
%    h(ii)     =   K/(2*f^4)*Y^3 + 3*K*thetaAir/(2*f^3)*Y^2 + (K*thetaAir^2-(f-a))/(f^2)*Y;
%    dhdy(ii)  = 3*K/(2*f^4)*Y^2 + 3*K*thetaAir/(f^3)*Y   +   (K*thetaAir^2-(f-a))/(f^2);
%    gdThe(ii) = 2*n^2/(c*phiThe(ii))*((f-a)*(phiThe(ii)-thetaAir)+f*h(ii));
%    dispersionThe(ii) = -2*n^4/(c*lambdaThe(ii)*phiThe(ii)^3)*((f-a)*thetaAir+f^2*
                                       \phiThe(ii)*dhdy(ii)-f*h(ii))*1000;
%end

%for ii = 1:noWvl
%    groupDelay(2*ii-1) = -(lambdaAir(ii)^2)/(2*pi*c)*(gamma(ii*res-(res-1)/2)-
                                       \gamma(ii*res-res+1))/(dlAir*(res-1)/2);
%    groupDelay(2*ii)   = -(lambdaAir(ii)^2)/(2*pi*c)*(gamma(ii*res)-
                                       \gamma(ii*res-(res-1)/2))/(dlAir*(res-1)/2);
%    lambdaGD(2*ii-1) = lambdaAir(ii) - (res-1)/4*dlAir;
%    lambdaGD(2*ii)   = lambdaAir(ii) + (res-1)/4*dlAir;
%end

tmp1 = groupDelay(1)-gdThe(1);
tmp2 = groupDelay(2*noWvl)-gdThe(noThe);
tmp3 = (tmp1+tmp2)/2;
groupDelay = groupDelay - tmp3;

for ii = 1:(noWvl)
    dispersionNum(ii) = (groupDelay(2*ii)-groupDelay(2*ii-1))/(dlAir*(res-1)/2)*1000;
end

%phi
%phiRelative


gdThe
groupDelay
dispersionThe
dispersionNum
```

cspecs.m
```matlab
% Computes performance specifications

bwl = 1;
bwh = 1;

ilambda = linspace(minLambda,maxLambda,200);
ilambda = transpose(ilambda);

exlAir = transpose(exlAir);

ieff = interp1q(exlAir,efficiency,ilambda);
ieff = 10*log10(ieff);

% Peak efficiency

maxEff = max(ieff(:,5))
```

79

```
for(ii = 1:190)
    if ((ieff(ii,5)<(maxEff-1))&(ieff(ii+10,5)>(maxEff-1)))
        bwl = ii;
    end
end

for(ii = 1:190)
    if ((ieff(200-ii+1,5)<(maxEff-1))&(ieff(200-ii-9,5)>(maxEff-1)))
        bwh = 200-ii+1;
    end
end

% Bandwidth in nm

bandwidth = (ilambda(bwh)-ilambda(bwl))*1000000000

bandCenter = round((bwh+bwl)/2);

for(ii = 1:(noThe-1))
    if ((ilambda(bandCenter)>=lambdaThe(ii))&(ilambda(bandCenter)<=lambdaThe(ii+1)))
        bandDisp = dispersionThe(ii);
        bcThe = ii;
    end
end

% Dispersion at center of band

bandDisp

% Standard deviation and normalized standard deviation of dispersion

standev  = std(dispersionThe((bcThe-10):(bcThe+10)),1)
nstandev = std(dispersionThe((bcThe-10):(bcThe+10))/dispersionThe(bcThe),1)

exlAir = transpose(exlAir);
```

plots.m

```
exlAirP = (exlAir-exlAir(exmidLambda))*1000000000;
lambdaGDP  = (lambdaGD -lambdaAir(midLambda))*1000000000;
lambdaAirP = (lambdaAir-lambdaAir(midLambda))*1000000000;
lambdaTheP = (lambdaThe-lambdaThe((noThe+1)/2))*1000000000;
TmainP = zeros(3,points*scale/32);
RmainP = zeros(3,points*scale/32);
yTP = zeros(1,points*scale/32);

for ii = 1:points*scale/32
    TmainP(1,ii) = Tmain((1+(res+1)/2),ii*32);
    TmainP(2,ii) = Tmain(exmidLambda,ii*32);
    TmainP(3,ii) = Tmain((noWvl*res-(res+1)/2),ii*32);
    RmainP(1,ii) = Rmain((1+(res+1)/2),ii*32);
    RmainP(2,ii) = Rmain(exmidLambda,ii*32);
    RmainP(3,ii) = Rmain((noWvl*res-(res+1)/2),ii*32);
    yTP(ii) = yT(ii*32);
end

TmainP = transpose(TmainP)
RmainP = transpose(RmainP)
yTP = transpose(yTP)

figure('PaperPosition',[2 1 4.5 9])
subplot(3,1,1)
plot(lambdaTheP,dispersionThe,'-',lambdaAirP,dispersionNum,'o','MarkerSize',4)
title(ttl)
```

```
ylabel('Dispersion (ps/nm)')
axis([exlAirP(1) exlAirP(noWvl*res) -7000 0]);
legend('Theoretical','Numerical',0);

subplot(3,1,2)
plot(exlAirP,10*log10(totalEff),'-',exlAirP,(max(10*log10(totalEff))-1)*ones(1,noWvl*res),':')
ylabel('Total Efficiency (dB)')
axis([exlAirP(1) exlAirP(noWvl*res) -10 0]);
legend('Total','-1dB',0);

subplot(3,1,3)
plot(exlAirP,10*log10(windowEff),'-',exlAirP,10*log10(plateEff),'-.',exlAirP,10*log10(lobe-
Eff),':',exlAirP,10*log10(couplingEff),'--')
ylabel('Efficiency Decomposition (dB)')
xlabel('Wavelength - Center Wavelength (nm)')
axis([exlAirP(1) exlAirP(noWvl*res) -10 0]);
legend('Window','Plate','Lobe','Coupling',0)

figure('PaperPosition',[2 1 4.5 9])
subplot(3,1,1)
plot(yTP,abs(TmainP(:,1)),'-',yTP,abs(RmainP(:,1)),':')

title(ttl)
ylabel('1549.7 nm Amplitude (a.u.)')
axis([0.02 0.08 0 0.06]);
legend('Tmain','Rmain',0)
subplot(3,1,2)
plot(yTP,abs(TmainP(:,2)),'-',yTP,abs(RmainP(:,2)),':')
ylabel('1550.0 nm Amplitude (a.u.)')
axis([0.02 0.08 0 0.06]);
subplot(3,1,3)
plot(yTP,abs(TmainP(:,3)),'-',yTP,abs(RmainP(:,3)),':')
xlabel('y (m)')
ylabel('1550.3 nm Amplitude (a.u.)')
axis([0.02 0.08 0 0.06]);

figure('PaperPosition',[1 1 6.5 9])
subplot(2,1,1)
plot(exlAirP,gamma,'x','MarkerSize',4)
title(ttl)
ylabel('Gamma (radians)')

subplot(2,1,2)
plot(lambdaTheP,gdThe*10^12,'-',lambdaGDP,groupDelay*10^12,'o','MarkerSize',4)
ylabel('Group Delay (ps)')
xlabel('Wavelength - Center Wavelength (nm)')
legend('Theoretical','Numerical',0)

diary off
```